1. Development of hybrid first principles – artificial intelligence models for high-temperature power systems

2025년 7월 7일 월요일 오전 11:39

1. Develop...

Applied Thermal Engineering 262 (2026) 124795

Contents lists available at ScienceDirect

Applied Thermal Engineering

journal homepage: www.elsevier.com/locate/apthermeng

Research Paper

Development of hybrid first principles – artificial intelligence models for transient modeling of power plant superheaters under load-following operation

Angan Mukherjee [a,1], Vivek Saini [a,1], Samuel Adeyemo [a,1], Debangsu Bhattacharyya [a,*], Daniel Purdy [b], Jonathan Parker [b], Charles Boohaker [c]

[a] Department of Chemical and Biomedical Engineering, West Virginia University, Morgantown, WV 26506-6070, USA
[b] Electric Power Research Institute, 1300 West WT Harris Blvd - Charlotte, NC 28262, USA
[c] Southern Company Services, Inc., 600 North 18th Street, Birmingham, AL 35203, USA

ARTICLE INFO

Keywords:
Hybrid model
Superheater
First-principles
Neural networks
Bayesian machine learning

ABSTRACT

This paper develops different approaches for synergistic integration of physics-based models with data-driven models for modeling of high temperature power plant superheaters. Two types of data-driven models are developed, namely all-nonlinear static-dynamic neural network models as well as models obtained using a Bayesian machine learning approach. Series, integrated, and parallel coupling of first-principles models and data-driven models are proposed. Algorithms for solving the training problems for the data-driven models and for simulation of the hybrid models are developed. The developed approaches are applied to high temperature power plant superheaters that face considerable modeling and measurement challenges. Measurement challenges arise due to harsh operating conditions that not only make placement of sensors difficult, but life of the placed sensors very limited. Modeling challenges arise due to complex inhomogeneous spatial distribution of flue gas and steam flowrates, especially under load-following operation and uncertainties in heat transfer characteristics because of multiple factors such as stochastic spatio-temporal variation of ash deposits on the superheater tubes in coal-fired power plants, internal oxide scale formation in the tubes, etc. First-principles two-dimensional differential-algebraic equation models of two industrial superheaters, one from a natural gas combined cycle plant and another from a coal-fired power plant, are developed. The results from the models are compared against industrial operational data. For all cases studied in this work, it is observed that both for steady-state and dynamic data, the hybrid models have much higher accuracy than when only the respective first-principles models are used. For example, during prediction of the average outside tube wall temperatures of superheater tubes at the combined cycle power plant, the root mean squared error observed for the standalone first-principles model improved from 12.3 °C to 0.5 °C post hybridization with data-driven models. Similarly, while predicting the main steam outlet temperature in the coal-fired plant, the hybrid models resulted in reduction of the root mean squared error value from 19.5 °C to around 2 °C. In addition, the hybrid models yield highly resolved spatio-temporal temperature profiles that can be helpful for developing monitoring approaches of these critical components under load-following operation.

1. Introduction

Superheaters are critical components in power plants for producing the main steam at the desired temperature. Under load-following operation, these high temperature components can suffer from considerable damage that can eventually lead to failure and thus can compromise the reliability of the power plants. This work investigates the use of hybrid models for spatio-temporal prediction of temperature in power plant superheaters.

Process systems can be modeled using first principles (FP) models based on conservation laws, material and thermodynamic properties, or using data-driven models based on measured operational data [1]. First-principles models can provide very good prediction even for cases where

* Corresponding author.
E-mail address: Debangsu.Bhattacharyya@mail.wvu.edu (D. Bhattacharyya).
[1] Angan Mukherjee, Vivek Saini and Samuel Adeyemo contributed equally to this work as joint first authors.

https://doi.org/10.1016/j.applthermaleng.2024.124795
Received 8 July 2024; Received in revised form 23 September 2024; Accepted 2 November 2024
Available online 6 November 2024

Nomenclature

A	total heat transfer area, m^2
c_p	specific heat capacity, kJ/kg. K
f	function of first principles model equations
g	function of data-driven model equations
h	convective heat transfer coefficient, KW/m^2. K
m	mass, kg
$\dot{m}$	total mass flow rate, kg/s
q	heat flux, KW/m^2
t	time, s
T	temperature, ° C
u	model input variables
v	velocity, m/s
v_p	valve opening
x	first principles model state variables
y	horizontal direction dimension/model output variables
z	vertical direction dimension

Greek Symbols

Δ	residuals
θ	parameters
ρ	density, kg/m^3

Subscripts

A,B,C,D	steam inlet pipe tags
avg	average
conv	convection
corr	correction
fg	flue gas
i	time step/inside
in	inlet
int	integrated
j	tube assembly/flow circuit number
meas	measured
mod	model
n	number
o	outside
opt	optimal
out	outlet
par	parallel
rh	reheater
st	steam
ser	series
spray	spray flow
tube	metal tube
wall	tube wall

Abbreviations

AI	artificial intelligence
ALAMO	automatic learning of algebraic models
ALVEN	algebraic learning via elastic net
ANN	artificial neural network
BIDASM	Bayesian identification of dynamic sparse algebraic models
BML	Bayesian machine learning
CNN	convolutional neural networks
DAE	differential algebraic equation
DABNet	decoupled A-B Network
DNN	deep neural networks
EM	expectation maximization
FP	first principles
GRU	gated recurrent unit
HP	high pressure
HRSG	heat recovery steam generator
LSTM	long-short term memory
MAIE	maximum absolute instantaneous error
ML	machine learning
NARX	nonlinear auto-regressive network with exogenous inputs
NGCC	natural gas combined cycle
NLD	nonlinear dynamic
NLS	nonlinear static
NN	neural network
ODE	ordinary differential equation
PDE	partial differential equation
PC	pulverized coal
RMSE	root mean square error
RNN	recurrent neural network
SINDy	sparse identification of nonlinear dynamics

there are no or limited data availability in certain range of operating conditions or for cases where data acquisition is not feasible given the current state of measurement technology. However, constructing accurate FP physics-based mechanistic models for complex nonlinear noisy dynamic systems may lead to excessive computational expense as well as challenging for online adaptation. Furthermore, it can also be difficult, if not impossible, to develop efficient physics-based models for certain complex phenomena that are poorly understood. In contrast, artificial intelligence (AI)/machine learning (ML) models are typically much faster in computation and can be relatively easier to develop, simulate, and adapt online, even for complex and ill-defined dynamic systems [2]. One of the primary limitations of the conventional data-driven models stems from the lack of predictive or extrapolative capabilities especially when there is information gap in the data used for model development. For example, high-temperature systems such as steam superheater systems have complex dynamics with limited measurements for key state variables like tube metal wall and flue gas temperatures [3]. Modeling such systems using either a standalone physics-based or AI model can yield inaccurate results. Hybrid models, however, synergistically combine FP models with AI models and can be leveraged to yield a monitoring framework that is adaptive, real-time, and accurate [4]. This work develops several approaches where first-principles mechanistic models developed for high temperature power plant superheaters [5] have been synergistically coupled with two different ML models, i.e., artificial neural networks [6] (ANN) and Bayesian Machine Learning [7] (BML) based approaches, thus exploiting their key strengths [8].

Over the last few decades, hybrid FP + AI models have found numerous implementations [9,10]. One of the most common applications of hybrid models has been in the form of lumped parameter models where AI models account for certain static process parameters to be subsequently utilized in the FP model [11,12]. Other implementations of hybrid FP + AI models include modeling of the residual from a FP model by using data-driven models applied on chemical reactors [13], energy systems [14], and biological approaches [15], physics informed machine learning approaches aimed at conservation of system physics represented by mass [16,17], energy [18], and momentum balances [19], and digital twin development for coal fired power plants [20,21] and biomass energy systems [22]. These models can lead to improved interpretability and efficient extrapolation capabilities [23,24]. There are significant opportunities, however, for exploiting the synergistic hybridization of FP models with data-driven models. For such hybrid models to be successful and yield desired outcomes, various other aspects need to be considered other than coupling approaches. In particular, it is important to consider what information needs to be exchanged

ABSTRACT

본 논문은 고온 발전소 과열기(superheater)의 모델링을 위해 물리 기반 모델(physics-based model)과 데이터 기반 모델(data-driven model)을 시너지 있게 통합하는 다양한 접근 방식을 개발하였다.
두 가지 유형의 데이터 기반 모델이 개발되었는데, 하나는 완전 비선형 정적-동적 신경망 모델(static-dynamic neural network model), 다른 하나는 베이지안 머신러닝(Bayesian machine learning) 기법을 통해 얻은 모델이다.
본 연구에서는 물리 모델(first-principles model, FP)과 데이터 기반 모델 간의 직렬(series), 통합(integrated), 병렬(parallel) 연결 구조가 제안되었으며, 각각의 구조에 대해 훈련(training) 알고리즘과 하이브리드 모델 시뮬레이션(simulation)을 위한 알고리즘이 개발되었다.
이러한 접근 방식은 고온 발전소 과열기 시스템에 적용되었으며, 해당 시스템은 모델링과 계측(measurement)에 있어 많은 어려움을 가지고 있다.
계측상의 문제는 고온 · 고압 운전 환경으로 인해 센서 설치가 어려우며, 설치된 센서의 수명도 매우 짧다는 데에서 발생한다.
모델링상의 문제는 특히 부하 추종(load–following) 운전 조건 하에서 배연가스(flue gas)와 증기 유량의 공간적 분포가 복잡하고 물리일하기 때문에 발생한다. 또한, 열전달 특성에 불확실성이 존재하는데, 이는 다음과 같은 다양한 요인에 기인한다:
예를 들어 석탄 화력 발전소에서는 과열기 튜브 외벽에 생기는 재(ash) 침전물의 시공간적 확률 분포, 튜브 내부의 산화물 스케일(oxide scale) 형성 등이다.
이에 따라, 천연가스 복합화력발전소와 석탄화력발전소의 실제 산업용 과열기를 대상으로 하는 2차원 물리 모델(2D differential-algebraic equation model)을 개발하였다.
개발된 모델 결과는 산업 현장의 운전 데이터와 비교되었으며, 모든 사례에 대해 다음과 같은 결과를 얻었다.
정상 상태(steady–state)와 동적(dynamic) 데이터 모두에서, 단독 물리 모델만 사용할 때보다 하이브리드 모델을 사용할 경우 예측 정확도가 크게 향상되었다.
예를 들어, 복합화력발전소에서 과열기 튜브의 외벽 평균 온도를 예측할 때, 물리 모델만 사용한 경우의 평균 제곱근 오차(RMSE)는 12.3도였으나, 데이터 기반 모델과 결합한 후에는 0.5도로 감소하였다.
또한 석탄화력발전소에서 메인 증기 출구 온도를 예측한 경우, 하이브리드 모델은 RMSE를 19.5도에서 약 2도로 줄였다.
뿐만 아니라, 하이브리드 모델은 시공간적으로 매우 세분화된(spatio–temporally resolved) 온도 분포를 제공할 수 있으며, 이는 부하 추종 운전 하에서 이와 같은 주요 구성 요소의 상태를 모니터링하는 방법을 개발하는 데 유용하게 활용될 수 있다.

between FP models and data-driven models and at what interval, how to select the specific data-driven model for the desired outcome, and when and how to adapt the hybrid model. Furthermore, if it is desired that both the FP and AI models represent nonlinear transients, then optimal synthesis of such hybrid models needs to consider complexity, computational expense, and accuracy.

For representing certain systems, more than one type of data-driven models may be simultaneously required in a hybrid framework [25]. The FP and data-driven models can be arranged in series or parallel or integrated or as combination of these configurations. If the FP model cannot adequately represent some phenomenon/phenomena of the process that is/are separable (i.e., neither the FP model impacts the results of the data-driven model, nor the data-driven model impacts the results of the FP model) and some or all of the inputs are used for both the FP and data-driven models, the parallel configuration is favoured [26,27]. The deficiencies in the FP model may be directly expressed by a data-driven model as a function of model inputs [28]. For non-separable discrepancies where either the FP model outputs serve as additional inputs to the data-driven model(s) or the data-driven model outputs serve as the additional inputs to the FP model inputs, but not both, then a series configuration is preferred. Series (or serial) configurations of FP with data-driven models have shown improved extrapolation properties as compared to the parallel architecture [29]. For non-separable discrepancies, where the FP model outputs serve as the (additional) inputs to the data-driven model and vice versa, then an integrated configuration is preferred. In the integrated approach, the results from the FP model are affected due to expected improved estimates of parameters/states, etc. from the data-driven model. It should be noted that the results from the FP model are not affected in the parallel configuration or in series configuration if the FP model precedes the data-driven model. The integrated approach has been often used in the existing literature for estimating time-invariant parameters [11,12] by a data-driven model to be utilized in the FP model. If the parameters to be estimated by the data-driven models are time-varying, then the integrated approach can lead to challenging training and/or adaptation problems for dynamical systems. Obviously, various combinations of series, parallel, and integrated configurations may be desired depending on the discrepancies of the data-driven model and FP model and their parameters. Furthermore, in all such approaches discussed in the literature, where certain process parameters for the FP model are estimated by a data-driven model, the training data for the respective AI models are generated by a first-order error backpropagation-based approach. While typically such algorithms for regression/optimization are computationally faster, the resulting training dataset may lack sufficient richness due to local approximation and absence of accurate Hessian information [30]. Therefore, for online applications, the hybrid models thus developed may require frequent retraining to ensure satisfactory predictive capabilities for highly nonlinear transient process systems for prolonged continuous durations of operation.

The objective of this work is to develop hybrid modeling approaches for predicting transient behavior of high temperature superheater components in power plant boilers. As the integration of renewables in the current energy grid is becoming prevalent worldwide to achieve low-carbon emissions, operation of existing fossil-fired power plants need to be flexible [31]. The current power generation fleet which is mainly designed for base load operations is facing several operational challenges due to these load-changing operations [32,33]. As a result, failure rate of the boilers especially that of the high temperature superheater components have gone up [34,35]. Advanced data-driven models utilising extensive operational datasets have been well developed and utilized in industrial plants for rotary equipment such as gas and steam turbines especially for monitoring of those equipment items. For static equipment such as boilers, limited tools are available commercially. For developing a monitoring framework for these components, reasonably accurate estimates of temperature profile with sufficient spatial resolution are needed since the metal temperature affects creep and fatigue damages [36] in boiler tubes and subsequent failure. However, it is challenging to develop accurate FP models for the superheaters due to multiple reasons. First of all, it is difficult to develop accurate models of the heat transfer characteristics in the superheater tubes due to build up of oxide scale inside the tubes [5]. The scale thickness keeps growing with time, but the scale can spall [37,38], which is highly stochastic. Furthermore, there is high uncertainty in the scale thermal characteristics [39,40]. In addition, in coal-fired power plants, there is deposit of coal fly ash on the outside of the tubes [41]. While frequent soot blowing is often used to clean those ash deposits, there may be fused ash that can be difficult to remove [42]. Thus, there is high uncertainty in the thickness and thermal characteristics of the ash deposit for coal-fired power plants. Second, modeling challenges for superheaters arise due to inhomogeneous spatial distribution of flue gas and steam flowrates, especially under load-following operation [43]. Due to the presence of thousands of tubes in this region and specific configuration of a given superheater, firing profile of the burners, etc., accurate dynamic modeling of flow inhomogeneity is challenging. Placing sensors in the superheater region is very challenging due to harsh operating conditions that not only make placement of sensors difficult [44], but life of the placed sensors are very limited especially in coal-fired boilers [45] where the superheater environment is highly erosive due to the fly ash-laden flue gas. Thus, developing hybrid models for the superheaters that can be eventually used for developing a monitoring framework is of high interest to utility operators.

Recently, a few hybrid modeling approaches have been implemented for process modeling, controls, and digital-twin development for thermal systems such as boiler and steam turbine for in-service power plants [20,46]. Other notable applications of hybrid models include tasks such as controlling fouling in biomass boilers [47] and performance enhancement of an ejector refrigeration system [48]. The hybrid models utilized in most of these works were a combination of lumped parameter physical mechanistic models and data-driven linear empirical models utilizing operational data. In particular, hybrid grey-box models have found implementations in industrial furnace systems [49], heat recovery steam generator (HRSG) [50] and various components of steam power plants (boiler, turbine, condenser, feed water system, etc.) [51,52]. The proposed models in these works generally used a combination of reduced order parametric models representing the physical system and static feedforward AI-based models for estimating unknown process parameters in thermal systems. Furthermore, grey-box modeling approaches for feedwater heater [53] and steam boiler system [54] have been developed by using detailed nonlinear FP differential algebraic equations (DAE) model based on mass and energy balances. The unknown system parameters were estimated for both the systems using nonlinear least-squares optimization utilizing operational measurement data. Similar approaches have been investigated for an electric hot water boiler system [55] and a superheater/reheater system in a combined cycle plant HRSG unit [56], using detailed mechanistic dynamic FP model based on differential mass and energy balance equations along with dynamic estimation of unknown heat transfer parameters. Dynamic hybrid models combining non-linear physics based models with gated recurrent unit (GRU) [14] or long-short term memory (LSTM) [57] type recurrent neural network (RNN) model have also been investigated for modeling heat absorption and fouling prediction in boiler systems. Recently, a hybrid modeling framework using dynamic models have been proposed for digital twin development in a coal-fired power plant [58]. The proposed model structure consists of FP based discrete-time model for different sections of the plant such as pulverizers, furnace, drum etc. along with LSTM type of RNN models for estimation of model parameters. Although many of such hybrid structurers utilizing dynamic AI models show satisfactory performance while representing critical process variables, the availability of limited transient operating data may lead to significant overfitting during model training, thus resulting in inferior predictive capabilities. Hybrid modeling techniques using lumped parameter physical models in addition to LSTM type RNNs

[59,60] and fuzzy logic based AI approaches [61] have also been used for superheater steam temperature control in industrial systems. More recently, a detailed dynamic distributed parameter model has been proposed for studying transient behavior of boiler systems under rapid load following operations [62]. The proposed models were validated using test data from an actual operating system showing its utility for simulating system behavior. Although most of the works referenced above have developed hybrid models of various components of thermal systems, most of these works have neither considered the spatial variability of process variables in the FP models nor the dynamics of time-varying parameters/variables that are represented by the AI models. Furthermore, a limited amount of operational dynamic data has been used for model validation in these works. An accurate prediction of the dynamic process variables and time-varying parameters for high temperature superheater systems is critical for developing a monitoring framework especially during load-following operations due to rapid changes in heat transfer performance and flow distribution during the transients.

The literature review on hybrid modeling of power plants identifies several gaps that we seek to fill in:

- Hybrid models of the superheater section of power plants using detailed distributed transient FP models along with dynamic data-driven models are currently not available.
- Modeling of time-varying parameters/variables by an AI model as part of the hybrid model for power plants has not currently been investigated. Moreover, the development of algorithms for generating training data during internal coupling between FP and AI models to address parametric uncertainties while ensuring sufficient data richness has not been explored.
- No hybrid model developed in existing literature provides estimates for the time-varying tube wall temperature profile in the superheater section of power plants.
- Main steam temperature is one of the most important variables for the power plant operation. A temperature that is higher than desired can cause significant damage to the steam turbine, while a temperature that is lower than desired can cause efficiency loss [56,63]. While the main steam temperature is a controlled variable and therefore measured, a predictive model can be helpful in developing a model-based efficient main steam temperature controller [56,63]. However, accurate prediction of the main steam temperature is difficult due to uncertain heat transfer characteristics, non-uniformity in flow direction, time-varying thermal holdup of the systems, etc. Hybrid models can be very useful for not only estimating the main steam temperature, but also other critical transient process variables such as metal wall temperatures of superheater tubes or flue gas temperatures, simultaneously. However, to the best of our knowledge, no work in existing literature discusses the development of a hybrid model for prediction of all these different types of transient temperature profiles (main steam, tube wall, flue gas) for pulverized coal (PC) or natural gas combined cycle plant (NGCC) power plants.
- Modeling spatio-temporal variability of temperature is critical for superheaters, where hybrid models can be particularly useful due to modeling and data challenges discussed before. We could not currently find any literature that has addressed this area.
- Model validation using experimental/industrial data has been generally done in the existing literature by using the steady-state data or dynamic data for a short operating range. It is desired that the models be validated in the expected range of power plant load and ramp rate as expected during the load-following operation..

This paper presents a systematic procedure for the selection of appropriate hybrid approaches for modeling of thermal systems in which dynamic industrial steam superheater systems for two different types of boiler systems were considered as case studies. The first system considered is part of an HRSG in a NGCC plant, and the other system is part of a PC power plant. In the present work, the FP models of both the industrial steam superheater systems which have been developed in our previous work [5] as two-dimensional (2-D) distributed DAE model considering differential mass and energy balance equations along with a detailed accounting of heat-transfer through the metal tube wall have been considered. For the ML models to be used for online applications, it is important to take into consideration contrasting advantages, and disadvantages of various types of AI-based modeling techniques. As potential candidate data-driven models in the hybrid FP + AI framework discussed in existing literature, different variants of deep neural networks (DNNs) are typically considered, such as LSTM [59,64] or GRU [14] types of RNNs, as well as convolutional neural networks [63] (CNNs). However, such conventional DNN models comprise significantly large numbers of parameters, thus leading to potential overfitting during model training especially in absence of large datasets [66,67]. Alternative data-driven approaches commonly used in hybrid FP + AI models involve derivative-free algorithms such as fuzzy logic based decision making [61], etc. However, such approaches may suffer from slow convergence in absence of sufficient exploration and exploitation of the solution space due to absence of gradient information during parameter estimation. Both of these AI-based models/approaches prove to be considerably challenging especially for the power plant superheaters for which large sized dynamic input/output data may not be available for model development. Our previous works have shown that sparse deterministic and probabilistic data-driven models significantly outperform several state-of-the-art approaches while modeling complex nonlinear chemical systems from noisy dynamic data typical of real plants. Drawing from those studies, in this work, the deterministic data-driven models are represented by hybrid all-nonlinear series/parallel static-dynamic neural networks [6] (referred to as 'NN' for the rest of the paper), while the probabilistic models are obtained from the BIDSAM (Bayesian Identification of Dynamic Sparse Algebraic Models) approach [7] (referred to as 'BML' for the rest of the paper). These models/algorithms consider a significantly lesser number of parameters (for sparse system identification) as compared to typical DNNs and hence correspond to much faster computation if the hybrid model needs to be retrained at frequent intervals during certain online applications. More details on the structurers and training algorithms for these specific data-driven models can be found in our previous papers [6,7]. While the NN models typically ensure faster computation and accurate model fit for highly nonlinear transient data, the BML models offer capabilities for handling noisy data and uncertainty quantification along with estimation of interpretable model parameters.

In summary, the major contributions of this paper are as follows:

- Three different structurers for integrating FP (physics-based) mechanistic models with data-driven models have been investigated – namely series, parallel and integrated configurations. In addition, series-parallel and integrated-parallel configurations are also investigated. Motivations for these structures are based on the evaluation of model discrepancies and analysis of how the FP and data-driven model can complement each other for achieving the desired model prediction performance.
- Novel hybridization approaches for exchange of appropriate information between FP and AI models have been developed with improved predictive and extrapolative capabilities while modeling industrial steam superheater systems under load-following conditions. Rigorous optimization-based algorithms are developed for generation of training data for AI models during internal synergistic coupling of FP and AI models, thus enhancing data richness for improved predictive capabilities. Another key focus is on developing predictive models for spatio-temporal variation of the main steam outlet temperature. In addition, predictive capabilities of the hybrid models for other variables of interest such as tube wall and flue gas temperatures are also evaluated. Accurately predicting the nonlinear

transient temperature profiles can be useful for developing a framework for monitoring damage accumulation in the systems under consideration.

- Two different types of sparse dynamic data-driven models with contrasting advantages and disadvantages are developed and analyzed in the hybrid FP data-driven modeling framework, namely the series/parallel all-nonlinear neural network models [6] and the BML models developed through BIDGAM algorithm [7]. These two approaches have been compared in terms of computational expense, predictive accuracy, model interpretability, sparsity, boundedness, and extrapolative capabilities while modeling the superheater systems. Two principal statistical measures that are considered for quantifying the relative performance of the proposed models are the root mean squared error (RMSE) and the maximum absolute instantaneous error (MAIE) calculated between the actual plant measurements and the predictions from the hybrid model.
- The proposed hybrid models have been developed and validated using dynamic data from the superheaters of two operating power plants- the first one being a part of an HRSG of a NGCC power plant and the other one being part of a PC-fired boiler unit. Prolonged durations of time-varying operational data under variable load conditions have been utilized for developing and validating the proposed hybrid modeling framework(s). As a measure of acceptability of the developed hybrid models, the maximum values of the RMSE and MAIE are set at 5 °C and 10 °C for both the NGCC and PC-fired power plants.

The rest of the paper is organized as follows. Section 2 includes brief discussions on the development of the individual components of the hybrid FP + AI models. The various model structures developed by synergistic coupling of FP and AI models are discussed in Section 3, whereas extensive descriptions of the two industrial superheater systems considered in this work have been included in Section 4. Section 5 presents a methodological workflow describing the interactions among different (FP and AI) models, while the results obtained from both the standalone FP as well as hybrid FP + AI models are presented in Section 6. Finally, the conclusions are presented in Section 7.

2. Hybrid model components

In this section, we provide brief discussions on the individual components of the hybrid models considered in this work. It may be noted that the various hybrid model components proposed in this work are generic and are flexible to be applied to model other complex nonlinear dynamic processes.

2.1. Dynamic FP model

The FP models implemented for modeling dynamic process systems can be typically derived from fundamental laws of physics, chemistry, thermodynamics, reaction kinetics and transport phenomena, such as mass, momentum, and energy balances. Such high-fidelity FP models can be developed in various mathematical forms. For example, as a system of algebraic equations, or a system of ordinary or partial differential equations (ODEs or PDEs), or a combination of both differential and algebraic equations leading to a generic nonlinear system of DAEs [5]. The physics-based mechanistic models developed for accurate process modeling have also traditionally shown significant efficiencies in predicting the thermo-physical properties of pure substances and their mixtures, especially for both reactive and non-reactive process systems.

The key advantages of using typical FP models over classical data-driven approaches for dynamic process systems are their predictive capability for process variables for which measurement data may not be available to develop data-driven model or data may be limited or may not be available for the desired spatial and temporal resolution. However, first-principles based modeling of complex nonlinear transient systems may face considerable difficulties. These generally stem either from the complex interactions underlying the physical phenomena or the lack of knowledge on system-specific mechanisms/nonlinearities, intermediates, high dimensionality, time-delay, and process uncertainties [13]. However, the overall predictive performance of a standalone FP model for such complex systems can be improved by combining physics-based knowledge with several AI approaches, thus leading to the development of different variants of hybrid FP + AI models (such as the various structures and approaches discussed in Section 3 of this paper).

2.2. ANN models

Conventional static feedforward neural networks are typically associated with inaccurate representations of temporal systems having time-lagged input variables [66,69]. On the other hand, although typical deep RNNs such as LSTMs, GRUs, etc. have shown improved performance while modeling transient systems [70,71], the presence of large numbers of hidden layers, and hence significantly large numbers of parameters, can lead to potential overfitting during model training [66,67]. A third type of neural network structure commonly used for modeling dynamic systems considers a linear dynamic model integrated with a nonlinear static neural network [72,73]. Such models may suffer from potential overfitting or excessive computational expense during parameter estimation, especially while modeling systems with highly nonlinear process dynamics [74] and may lead to relatively high instantaneous errors. Our previous work [6] has shown that series and parallel all-nonlinear architectures combining a nonlinear static (NLS) NN with a nonlinear dynamic (NLD) NN significantly outperforms several existing state-of-the-art models such as LSTM, GRU, Decoupled A-B Network (DABNet)[72] in terms of prediction accuracy and computational expense while modeling complex nonlinear dynamic systems.

For the hybrid all-nonlinear series/parallel static-dynamic neural networks considered in this work, the NLS model is represented by a three-layered feedforward neural network [75] whereas, the NLD model refers to a Nonlinear AutoRegressive with eXogenous inputs (NARX) type of RNN [76,77]. Obviously, any other type of static and/or dynamic neural network model can readily be considered as well in this framework. For the all-nonlinear series configuration, two different architectures are possible: the NLS followed by the NLD model (denoted by 'NLS – NLD' type network) and the NLD followed by the NLS model (denoted by 'NLD – NLS' type network). The all-nonlinear parallel configuration involves the NLS and NLD models arranged in parallel with one another, subject to the same set of model inputs. The block-oriented structures of the all-nonlinear series and parallel network models have been shown in Fig. 1. For simplicity, the optimal model among the hybrid series and parallel all-nonlinear static-dynamic neural networks for every different implementation case study under consideration has been referred to as 'NN' for the rest of the paper.

Training the hybrid all-nonlinear static-dynamic networks can be difficult and computationally expensive, especially while trying to simultaneously estimate the optimal parameters of both static and dynamic networks in a monolithic approach. Our previous work [6] discussed the development of sequential decomposition-based algorithms by exploiting the network structures for training the static-dynamic models which have shown to achieve convergence 50–100 times [6] faster than the monolithic (simultaneous) parameter estimation approaches. The codes for training and simulating the hybrid all-nonlinear static-dynamic network models are also publicly available at: https://github.com/mukherjeeangan20/Hybrid_StaticDynamic_NN_Models.

2.3. BML models

The black box nature of most data-driven models leads to the major

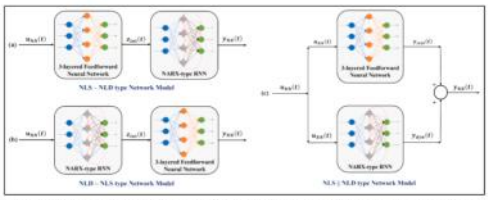

Fig. 1. Block-oriented structures for (a) NLS-NLD (series), (b) NLD-NLS (series) and (c) NLS||NLD (parallel) types of hybrid all-nonlinear static-dynamic networks.

drawback of lack of model interpretability consequent upon the complex structures of the underlying models. While our previous work [6] has addressed the issue of sparsity in the use of conventional ANN/NN, several works exists that attempt to address the challenge of model interpretability including Sparse Identification of Nonlinear Dynamics (SINDy)[78], Automatic Learning of Algebraic Models (ALAMO)[79] and Algebraic learning via elastic net (ALVEN)[80]. While these approaches give functional relationships between input and output variables, they have mainly been tested on synthetic data that are noise-free. In our previous work [7], we have shown, for some specific case studies, the ALAMO and SINDy algorithms are sensitive to the presence of noise in the training data. This significantly influences the model size and prediction accuracy for the algorithms. On the contrary, our developed BIDGAM algorithm [7] demonstrates significant robustness to noise as model size, model form, and prediction accuracy remain consistent whether model is developed using 'true' or noisy data. The BIDGAM algorithm achieves model interpretability (i.e., an understanding of the causation and effect of the input variables on the output variables) by approximating system nonlinearities by a combinations of a set of well-defined basis functions. These basis functions are obtained from linear and nonlinear transformations of the input variables and their interactive effects with the measurements. The selection of the optimal subset of the resulting large family of basis functions is done by using a branch and bound algorithm. Candidate models are compared using an information criterion that rewards model fitness, penalizes model size and complexity, while also incorporating a measure of parameter estimability (i.e., the ability to identify unique values for the model parameter from the available data) into the process. Robustness of this algorithm to noise is enhanced by explicitly accounting for noise and their possible correlation during parameter estimation which employs the two-step procedure of an expectation maximization (EM) algorithm. The efficiency of this algorithm makes it suitable for model development by using the real plant data such as from the industrial superheater systems that are typically corrupted with noise of unknown characteristics. The codes for BIDGAM algorithm for developing sparse steady-state and dynamic data-driven models are publicly available at: https://github.com/adityaure/BIDGAM_Codes.

3. Configurations of hybrid FP + AI models

This section discusses each hybrid FP + AI model architecture proposed in this paper and the motivation behind transfer of appropriate information to and from each FP and AI models while constructing accurate hybrid models for various dynamic process systems. It is to be noted that a particular hybrid model structure is neither specific nor exclusive to the corresponding implementation discussed in this paper. Obviously, one or more structures proposed in this work can be applied to a particular objective subject to availability of necessary data. Although theoretically all structures are expected to be accurate for unanticipated operations, this paper presents a systematic approach of selecting the optimal hybrid FP + AI model for representing key variables of interest.

3.1. Series hybrid FP + AI model

A possible configuration of the series hybrid FP + AI model is shown in Fig. 2. Obviously, the AI model can precede the FP model, or the FP model can be sandwiched between two AI models or other way round and there can be many such series of FP and AI models that can be considered. Additional synthetic inputs to the hybrid model may be the same ($u_i(t)$) and/or different ($u_{i,FP}$) as compared to the inputs to the FP model (refer Fig. 2). θ_{FP} and θ_{AI} refer to the model parameters for the FP and AI models, respectively, whereas $Y_{i,FP/AI}(t)$ represent the final outputs from the overall hybrid model. It should be noted that for this specific structure of the hybrid model, the model structure, i.e., the arrangements and interactions between the FP and AI model, remain consistent during both training and validation (simulation) of the hybrid FP + AI models. This may not be the case for the other structures proposed in this work. The dynamic target outputs for the AI models are considered as the residuals ($\Delta_i(t)$) calculated between the measured values $\left(Y_{i,meas}(t)\right)$ and the FP model predicted values $\left(Y_{i,FP}(t)\right)$ of the i^{th} output variable, as defined by Eq. (1), for the final superheater systems under consideration.

$$\Delta_i(t) = Y_{i,meas}(t) - Y_{i,FP}(t) \tag{1}$$

3.2. Integrated hybrid FP + AI model

The flow of information between the FP and AI models in the hybrid framework does not need to be one directional. For some applications, it may become necessary that information gets exchanged internally between the two models, as shown in Fig. 3. Such types of integrated cross-coupling configurations may be necessary to handle uncertainties in process parameters considered in the FP model. However, unlike the series hybrid FP + AI model discussed in Section 3.1, the integrated hybrid FP + AI model structure may slightly change during training

3. 하이브리드 FP + AI 모델의 구성

이 장에서는 본 논문에서 제안한 **각 하이브리드 FP(물리 기반 모델) + AI(인공지능) 모델 구조**와, 다양한 동적 공정 시스템(dynamic process systems)에 대해 **정확한 하이브리드 모델을 구축할 때 FP 모델과 AI 모델 간에 적절한 정보를 주고받아야 하는 이유**(중기)에 대해 논의한다.

특정 하이브리드 모델 구조는 본 논문에서 논의된 구현에만 독화되거나 독점적인 것이 아님을 주목할 필요가 있다.
명확히 말하자면, 본 연구에서 제안된 하나 이상의 구조는 필요한 데이터가 확보된다면 특정 목적에 적용될 수 있다.
이론적으로는 모든 구조가 예기치 않은 운전 조건에서도 정확한 것으로 예상되지만, 본 논문에서는 주요 관심 변수들을 나타내기 위해 최적의 하이브리드 물리 모델(FP, first−principles model) + 인공지능(AI) 모델을 선택하는 체계적인 접근 방식을 제시한다.

3.1. 직렬 하이브리드 FP + AI 모델 (Series hybrid FP + AI model)

직렬 하이브리드 FP + AI 모델의 가능한 구성은 Fig. 2에 제시되어 있다.
AI 모델이 FP 모델보다 앞에 배치될 수도 있고, FP 모델이 두 AI 모델 사이에 위치할 수도 있으며, 그 반대의 경우도 가능하다.
이와 같이 여러 개의 FP와 AI 모델이 직렬로 연결된 다양한 구조가 고려될 수 있다.
하이브리드 모델에 대한 추가 합성 입력(synthetic inputs)은 동일한 입력 $u_i(t)$일 수도 있고, FP 모델에 대한 입력과는 다른 $u_{i,FP}$일 수도 있다 (Fig. 2 참조).
모델 파라미터 θ_{FP}와 θ_{AI}는 각각 FP 모델과 AI 모델의 파라미터를 의미하며, $y_{i,FP/AI}(t)$는 전체 하이브리드 모델의 최종 출력을 나타낸다.
이 하이브리드 모델 구조에서는, 훈련(training)과 검증(validation, 시뮬레이션) 단계 모두에서 FP 모델과 AI 모델의 배치 및 상호작용 방식이 동일하게 유지된다는 점에 유의해야 한다.
이것은 본 논문에서 제안한 다른 구조들에는 해당되지 않을 수 있다.
AI 모델의 동적 목표 출력(dynamic target outputs)은 측정값 $y_{i,meas}(t)$과 FP 모델 예측값 $y_{i,FP}(t)$ 간의 차이인 잔차 $\Delta_i(t)$로 간주된다.
이 관계는 최종 과열기(superheater) 시스템에 대해 다음과 같이 정의된다.
$\Delta_i(t) = y_{i,meas}(t) - y_{i,FP}(t)$ (식 1)

3.2. 통합형 하이브리드 FP + AI 모델 (Integrated hybrid FP + AI model)

하이브리드 프레임워크에서 FP 모델과 AI 모델 간의 정보 흐름은 반드시 단방향일 필요는 없다.
일부 응용에서는 Fig. 3에 나타난 바와 같이, 두 모델 사이에서 내부적으로 정보가 교환되어야 할 필요가 있을 수 있다.
이러한 형태의 통합된 교차 연결 구조(integrated cross−coupling configurations)는 FP 모델에서 고려된 공정 파라미터의 불확실성을 처리하는 데 필요할 수 있다.
그러나 3.1절에서 논의한 직렬 하이브리드 FP + AI 모델과는 달리, 통합형 하이브리드 FP + AI 모델의 구조는 훈련(training)과 시뮬레이션(simulation) 단계에서 약간 달라질 수 있다.
이는 Fig. 3(b)의 점선 화살표로 표현된 것처럼, FP 모델에서 AI 모델로 어떤 정보가 전달되는지에 따라 결정된다.

특정 하이브리드 모델 구조가 본 논문에서 제시된 구현 사례에만 국한되거나 독점적인 것은 아니라는 점에 주목할 필요가 있다.
즉, 이 논문에서 제안된 여러 구조들 중 하나 이상은, 필요한 데이터만 갖춰진다면 다양한 목적에 맞게 적용할 수 있다.
이론적으로는 어떤 구조든 예기치 않은 운전 상황에서도 정확한 결과를 낼 것으로 기대되지만,
본 논문에서는 관심 있는 주요 변수들을 잘 표현할 수 있도록 **최적의 하이브리드 모델** — 즉, 물리 기반 모델(FP, first−principles model)과 인공지능 모델(AI)을 결합한 모델 — 을 **선택하는 체계적인 방법**을 제시한다.

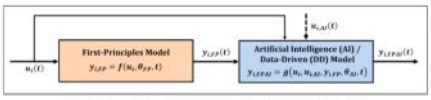

Fig. 2. Block-oriented configuration of serial hybrid FP + AI model during training and simulation.

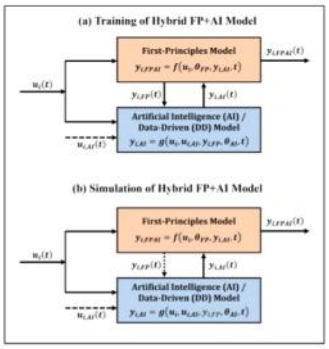

Fig. 3. Block-oriented configurations of integrated hybrid FP + AI model during (a) training and (b) simulation.

versus simulation depending on what information gets exchanged from the FP to the AI models (represented by the dotted arrow in Fig. 3 (b)). While a solid arrow in Fig. 3 (a) signifies that the transfer of information from the FP to AI models is mandatory during development (training) of optimal hybrid models, such transfer may not always be necessary during model simulation, as represented by the dotted arrow in Fig. 3 (b). For the case when the AI models utilize the instantaneous outputs of the standalone FP model as additional (synthetic) inputs during model training followed by subsequent transfer of information back to the FP model, the algorithm follows the same sequence even during simulation, i.e., when the optimally trained model is considered for future prediction subject to unknown inputs. In such examples, at every time step, the original FP model is solved first, followed by transferring partial or total information about the FP models' outputs to the AI models. Thereafter, the data-driven models utilize all information obtained from the FP model, along with additional inputs, if necessary, before sending back corrected estimates of certain parameters with which the FP model is simulated for a second time (within the same iteration/time index) leading to the final outputs $\left(y_{1,FPAI}\right)$ from the overall hybrid model.

The integrated arrangement of FP and AI models may also have certain specific applications, where the AI models do not require instantaneous estimates of any variable from the FP model as additional inputs during their training. In such examples, even though partial information from the FP model may get transferred to the AI models during training, such information is only utilized for data preparation for the AI models, i.e., not as additional inputs. Therefore, although the sequential integrated framework holds true during training/development of the hybrid model, the model architecture transforms to a series configuration during model simulation. At every time step during simulation of the optimal hybrid model, the AI models are first simulated followed by the FP model which can directly utilize the corrected parametric estimates transferred from the simulation of the optimal AI models. This second approach (i.e., considering $y_{1,FP}$ only for data preparation for AI models instead of additional inputs) also reduces the number of function evaluations during forward simulation of the integrated hybrid FP + AI models when exposed to unknown inputs, since it involves the FP model to be solved only once, thus leading to relatively faster computation as compared to the first approach (i.e., considering $y_{1,FP}$ as additional inputs for the AI models) where the FP model has to be solved twice during each iteration/time step.

3.2. Parallel hybrid FP + AI model

The parallel arrangement of FP and AI models become necessary for various applications, where even though a mechanistic (FP) model is available, its predictive capabilities are limited due to inaccurate descriptions of certain effects, nonlinearities, or dynamic behavior. The fundamental difference of this type of configuration with the previous two structures described in Sections 3.1 and 3.2 is that the parallel hybrid FP + AI model provides the flexibility of optimal synthesis of both FP and AI models independently without requiring sequential transfer of any information from one to another or between each other, as shown in Fig. 4. However, partial or total information may be transferred from the FP to AI models during training the parallel hybrid FP + AI model (denoted by the dotted arrow in Fig. 4 (a), but such information will only be used in preparing input–output data for the data-driven models. The outputs of the data-driven models, for this configuration, act as additive corrections or augmentations of those obtained from the FP model, thus leading to the generation of the overall outputs from the parallel hybrid FP + AI model represented by $y_{1,FPAI}(t)$.

It is to be noted that depending on the specific application of the hybrid model, the parallel structure can accommodate various model forms substituting the FP and/or AI models. For example, the series hybrid FP + AI model (as described in Section 3.1) can readily replace the FP model in the parallel framework, thus leading to a 'series–parallel hybrid FP + AI model'. Similarly, if the FP block in the parallel structure gets substituted by the integrated hybrid FP + AI model (as discussed in Section 3.2), it may lead to the 'integrated-parallel hybrid FP + AI model' architecture. The corresponding architectures of series–parallel and integrated-parallel hybrid models during simulation have been shown in Fig. 5, where $y_{1,FPAI_s}$, $y_{1,FPAI_p}$ and $y_{1,FPAI_{ip}}$ refer to the outputs from the series, integrated, and parallel hybrid FP + AI models, respectively. The training algorithms also follow similar structural representations.

4. Applications of hybrid models to industrial steam superheater systems

This section briefly describes the geometrical configurations and the detailed dynamic first principles model development for two industrial steam superheater systems considered in this work for the validation of the hybrid modeling framework. The first system, referred to as 'Plant A' for the remainder of this paper, is a final superheater system that is part of an HRSG unit in an NGCC plant. The second system, referred to as 'Plant B' for the remainder of this paper, is another final superheater system which is part of a PC-fired boiler unit. Two different types of superheater systems have been selected in this study to demonstrate the applicability of the proposed hybrid models to model any generic system using different types of fuels for combustion. Plant A superheater system uses natural gas fuel while Plant B utilizes solid pulverized coal for combustion. The use of a gaseous or solid fuel for combustion leads to a direct impact on the performance and efficiency of the system. The operating temperature of gas fired systems are usually lower with steady operating conditions because of less impurities in natural gas. On the other hand, solid fuel fired systems operate at higher temperatures with frequent fluctuations in operating conditions due to the presence of ash and soot in the solid fuel. Hence, the dynamic behavior of the two systems are quite different from each other. Therefore, the development of hybrid models for these two systems will be quite challenging and will help in establishing the robustness of the proposed hybrid modeling framework.

Fig. 4. Block-oriented configurations of parallel hybrid FP + AI model during (a) training and (b) simulation.

Fig. 3(a)와 실선 화살표는 최적의 하이브리드 모델을 개발(훈련)하는 동안 FP 모델에서 AI 모델로 정보가 전달되는 것이 필수적임을 의미한다.
반면 Fig. 3(b)의 점선 화살표로 나타낸 바와 같이, 시뮬레이션 단계에서는 이러한 정보 전달이 항상 필요하지 않을 수 있다.
AI 모델이 훈련 과정에서 독립형 FP 모델의 순간적인 출력 값을 추가적인 합성 입력(synthetic input)으로 활용한 다음, 그 정보를 다시 FP 모델로 전달하는 방식일 경우, 시뮬레이션 단계에서도 동일한 순서를 따른다.
즉, 최적 훈련된 모델이 향후의 예측(future prediction)을 위해 미지의 입력값에 적응할 때도 동일하게 처리된다는 의미다.
이러한 예시에서 매 시간 스텝마다 먼저 기존의 FP 모델이 해결되고, 이후 제한 추측 정보의 일부 또는 전체가 AI 모델로 전달된다.
그 다음, 데이터 기반 모델(data–driven model)은 필요 시 추가 입력과 함께 FP 모델로부터 받은 모든 정보를 활용한 후, 특정 파라미터에 대한 보정 추정값(corrected estimates)을 다시 FP 모델로 전달한다.
FP 모델은 같은 반복/시간 인덱스 내에서 이 보정된 파라미터를 사용해 두 번째로 시뮬레이션이 수행되며, 이 과정을 통해 하이브리드 모델의 최종 출력인 $y_{1,FPAI}$가 도출된다.

FP 모델과 AI 모델을 통합한 구성(integrated arrangement)은 다음과 같은 특정한 응용 문야에도 적용될 수 있다.
즉, AI 모델이 훈련 중에 FP 모델의 어떤 변수에 대한 순간적인 추정값을 추가 입력으로 필요로 하지 않는 경우이다.
이러한 예시에서는, FP 모델로부터 일부 정보가 AI 모델로 전달되기는 하지만, 그 정보는 오직 AI 모델을 위한 데이터 준비(data preparation) 용도로만 사용되고, 직접적인 추가 입력으로는 사용되지 않는다.
따라서 하이브리드 모델의 훈련 또는 개발 단계에서는 통합형 프레임워크 구조가 유지되지만, 모델 시뮬레이션 단계에 접어가면 모델 구조가 직렬(series) 구성으로 바뀌게 된다.
최적화된 하이브리드 모델의 시뮬레이션이 진행되는 동안, 매 시간 스텝마다 먼저 AI 모델이 실행되고, 이어서 FP 모델이 실행된다.
이때 FP 모델은, 앞서 AI 모델 시뮬레이션 결과로부터 전달된 보정된 파라미터 추정값(corrected parametric estimates)을 직접 활용하여 계산된다.

이 두 번째 방식(즉, $y_{1,FP}$를 AI 모델의 추가 입력으로 사용하는 대신, 데이터 준비 단계에만 활용하는 방식)은 향후 예측 시 동적형 하이브리드 FP + AI 모델의 전방 시뮬레이션(forward simulation) 동안 함수 계산 횟수를 줄여주는 효과가 있다.
이는 FP 모델을 한 번만 계산하면 되기 때문이며, 그 결과 첫 번째 방식(즉, $y_{1,FP}$를 AI 모델의 추가 입력으로 활용하여 매 반복 또는 시간 스텝마다 FP 모델을 두 번 계산하는 방식)에 비해 상대적으로 계산 속도가 빨라진다.

3.3. 병렬 하이브리드 FP + AI 모델

FP 모델과 AI 모델을 병렬로 구성하는 방식은 다양한 응용 문야에서 필요해진다.
이 경우에는 기계적(물리 기반) 모델(FP)이 존재하더라도, 특정 효과나 비선형성, 혹은 동적 거동(dynamic behavior)을 정확히 설명하지 못해 예측 능력이 제한적일 수 있기 때문이다.
이 구조가 3.1절과 3.2절에서 설명된 앞선 두 구조와 본질적으로 다른 점은 다음과 같다.
병렬 하이브리드 FP + AI 모델은 FP 모델과 AI 모델 사이에 정보 전달 순서를 요구하지 않고, 각 모델을 독립적으로 최적 구성(optimal synthesis)할 수 있는 유연성을 제공한다 (Fig. 4 참조).
다만, 훈련 단계에서는 Fig. 4(a)의 점선 화살표로 나타낸 것처럼 FP 모델에서 AI 모델로 일부 또는 전체 정보가 전달될 수 있다.
하지만 이 정보는 어디까지나 데이터 기반 모델(data–driven model)을 위한 입력–출력 데이터 구성에만 사용된다.
이 구성에서 데이터 기반 모델의 출력은 FP 모델 결과에 보정 또는 보완(additive correction or augmentation)을 더하는 방식으로 동작하며, 그 결과로 병렬 하이브리드 FP + AI 모델의 전체 출력 $y(t)$가 생성된다.
또한, 하이브리드 모델의 구체적인 적용 목적에 따라, 병렬 구조는 FP 모델 또는 AI 모델을 다양한 형태의 모델로 대체할 수 있는 유연성을 제공한다.
예를 들어, 3.1절에서 설명된 직렬 하이브리드 FP + AI 모델(series hybrid FP + AI model)은 병렬 프레임워크 내의 기존 FP 모델을 쉽게 대체할 수 있으며, 이로써 '직렬–병렬 하이브리드 FP + AI 모델(series–parallel hybrid FP + AI model)' 이 된다.
마찬가지로, 병렬 구조에서의 FP 블록이 3.2절에서 설명된 통합형 하이브리드 FP + AI 모델(integrated hybrid FP + AI model)로 대체된다면, 이는 '통합–병렬 하이브리드 FP + AI 모델(integrated–parallel hybrid FP + AI model)' 구조로 이어진다.
이러한 직렬–병렬 및 통합–병렬 하이브리드 모델의 시뮬레이션 구조는 Fig. 5에 제시되어 있으며,
여기서 $y_{1,FPAI_s}$, $y_{set\_i,FPAI_p}$, $y_{int_i,FPAI_par}$는 각각 직렬, 통합, 병렬 구조의 하이브리드 FP + AI 모델에서의 출력값을 의미한다.
각 구조에 대한 훈련 알고리즘 또한 이와 유사한 구조 표현을 따른다.

4. 산업용 증기 과열기 시스템에 대한 하이브리드 모델 적용

이 절에서는 본 논문에서 제안된 하이브리드 모델링 프레임워크의 유효성을 검증하기 위해 고려된 두 개의 산업용 증기 과열기 시스템에 대해, 그 **↑↓기하학적 구성(geometrical configuration)↑↓**과 **동적 물리 모델(first–principles model)** 개발 내용을 간략히 설명한다.
첫 번째 시스템은 '**Plant A**'로 명명되며, 이는 NGCC(natural gas combined cycle) 발전소의 HRSG(폐열 열회수 보일러) 유닛에 속하는 **최종(superheater) 과열기 시스템**이다.
두 번째 시스템은 '**Plant B**'로 명명되며, 이는 PC–fired boiler(분말 석탄 연소 보일러) 유닛에 속한 또 다른 최종 과열기 시스템이다.
이 연구에서는 서로 다른 연료를 사용하는 **두 가지 유형의 과열기 시스템**을 선정하여, 제안된 하이브리드 모델이 다양한 연소 연료를 사용하는 **일반적인 엔시스템에 적용 가능함을 입증**하고자 하였다.
Plant A는 천연가스(natural gas)를 연료로 사용하고, Plant B는 고체 분쇄 석탄(pulverized coal)을 연료로 사용한다.
연소에 사용되는 연료가 기체(gaseous)인지 고체(solid)인지에 따라, 시스템의 성능과 효율에 **직접적인 영향**을 미친다.
예를 들어, 천연가스를 사용하는 시스템은 불순물이 적기 때문에 일반적으로 **운전 온도가 낮고 운전 조건이 안정적**이다.
반면, 석탄을 사용하는 시스템은 불순물이 많고 연소 특성의 불확실성도 크기 때문에, **운전 온도가 높고 동적 변동성이 크며**, 운전 조건 또한 더 가변적이다.

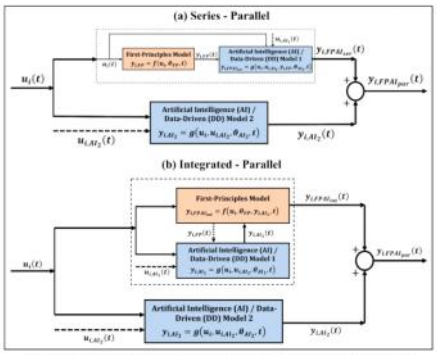

Fig. 5. Block-oriented configurations of (a) series–parallel and (b) integrated-parallel hybrid FP + AI models during simulation.

other hand, the solid coal fired systems experiences high operating temperatures with more dynamic variability in operating conditions because of large amount of impurities and uncertainties associated with a solid combustion fuel. Hence, to study the performance of hybrid models over a variety of different operating conditions and system characteristics, two different types of superheater systems have been used in this work. Operational data is available for both the units from the industrial partner plants which have been utilized for the

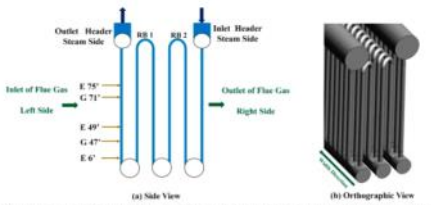

Fig. 6. Final superheater system (Plant A) layout (a) side view (marked locations on the left side indicate elevation in ft) and (b) Orthographic view (three-dimensional) schematic of tube assemblies.

마라서 다양한 운전 조건과 시스템 특성에서 하이브리드 모델의 성능을 연구하기 위해, 본 연구에서는 두 가지 유형의 superheater(과열기) 시스템을 사용하였다.

그림 6. 최종 superheater(과열기) 시스템 (플랜트 A) 배치도
(a) 측면도 (운전에 표시된 위치는 높이(ft)를 나타냄)
(b) 튜브 조립체의 정사영(삼각형) 개략도

두 과열기 시스템 모두에 대해 산업 파트너 플랜트로부터의 운전 데이터가 제공되어 있으며, 이는 제안된 하이브리드 FP + AI 모델의 개발 및 검증에 활용되었다.

development and validation of the proposed hybrid FP + AI models.

4.1. Plant A final superheater system (HRSG-NGCC Unit)

The power plant (Plant A) system is a final superheater system which is part of an HRSG unit in an NGCC plant having a rated capacity of 600 MW. The layout of the selected system is shown in Fig. 6. The main steam produced from the superheater system is transported to an outlet steam header connected to the main steam pipeline which connects further to the high-pressure (HP) steam turbine. The main steam outlet conditions of the superheater are 536 °C and 10 MPa under nominal conditions.

In Fig. 6 [a], the side view of the system is represented schematically. The system consisting of a six-pass tube assembly configuration where the steam enters through the inlet header on the upper right side of the diagram and exits through the outlet header depicted on the upper left side of the diagram. Furthermore, the actual system contains a total of 74 flow circuits along the width direction as shown in Fig. 6 (b) with an orthographic view of the superheater system. Each of these flow circuits is formed by the combination of the six-pass tube assembly shown in Fig. 6 (a), arranged behind one another in a staggered arrangement. An extensive amount of temperature measurement data was available for this system from thermocouples placed at the locations marked in Fig. 6 (a). In total out of the 74 flow circuits, these thermocouples were placed on 18 flow circuits making the system well instrumented as compared to typical power plant superheater systems. The thermocouples placed on these 18 flow circuits at various locations (refer Fig. 6 (a)) are categorized into two types. The first ones are thermocouples for measuring outer diameter tube wall temperatures. These thermocouples are denoted by E 6', E 49', E 75', RB 1, and RB 2 and are welded to the outside tube wall surface. The second ones are thermocouples for measuring the flue gas temperatures. These thermocouples are denoted by G 47' and G 71'. They are placed by resting them on tube supports and not attached directly to the tube wall surface. The numerical value in each location tag describes the height at which the sensor is placed. The main steam temperature measurement, which is an average of the steam temperatures at the header outlet is also available for this system. In addition, the inlet flue temperature measurement along the flue gas flow path on the left side as shown in Fig. 6 (a) is also available for this system from the plant operating data. A set of four thermocouples located on the left side of the HRSG at the upstream of the final superheater is utilized to calculate the mean for the inlet flue gas temperature which is then used in the hybrid model as input data.

4.2. Plant B final superheater system (PC-fired power plant boiler)

The second final superheater system (Plant B) analyzed in this study is part of a PC-fired power plant boiler with a generating capacity of 786 MW. The PC boiler first bituminous coal via six pulverizers, producing main steam at nominal conditions of 537 °C and 27 MPa. The configuration of the selected superheater system is shown in Fig. 7. The system consists of a two-pass tube assembly arrangement. Each pass of the given system consisted of six individual tubes, configured as a vertical outlet from the first header, with a 180° smooth transition followed by a vertical section into the outlet header. It should be noted that the schematic diagram in Fig. 7. shown the transitions as angular rather than smooth assembly configuration) for ease of illustration. The six individual tubes are numbered as T1 to T6 from right to left as shown in Fig. 7, with T1 being the longest and T6 the shortest in the flue gas path which flowed horizontally from right to left side as depicted in Fig. 7. Also, along the flue gas path, T1 is the first and last tube, while T6 tube is the innermost tube exposed to flue gas flow. The steam enters the system from the inlet header on the upper right-side section flowing down vertically with equal distribution into the six shaped tubes and exits the superheater system through the outlet header on the upper left-side section where all six tubes were welded. The outlet steam header connects further to the main steam line which connects to the HP steam turbine. The layout in Fig. 7 is the side view of the system. The entire final superheater system consisted of [30" identical flow assemblies, each with six U-tubes with a two-pass tube arrangement as shown in Fig. 7, stacked one behind another. This system was also uncharacteristically well instrumented, with the capability including 75 thermocouples in the penthouse attached to measure tubing across the width of the boiler aligned with selected assemblies' tube-to-header connections to the outlet header. However, the inlet temperature for the flue gas side (right side, as shown in Fig. 7) for this system is only available for a limited time duration from the plant historian and not for the entire duration which is needed for the model simulation. Hence, using the limited dataset, a quadratic correlation has been developed for representing the flue gas inlet temperature as a function of gross plant load (MW) and this correlation is then used for simulation of the entire dataset. It is observed that the data obtained for the superheater system from this PC-fired boiler system

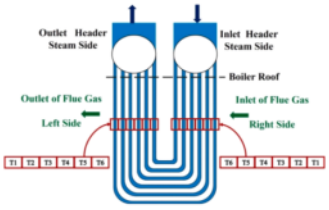

Fig. 7. Final superheater system (Plant B) layout. Note: the actual tube arrangement involves smooth transitions rather than the angular transitions shown in the schematic diagram.

4.1. 플랜트 A 최종 superheater(과열기) 시스템 (HRSG–NGCC 유닛)

플랜트 A는 HRSG(Heat Recovery Steam Generator, 열회수 증기발생기) 유닛의 일부로 구성된 최종 superheater 시스템이며, 600 MW의 정격 용량을 가지는 NGCC(Natural Gas Combined Cycle, 천연가스 복합화력발전) 발전소에 속한다. 선택된 시스템의 배치는 그림 6에 나타나 있다. superheater 시스템에서 생성된 주증기는 출력 steam header(스팀 헤더)를 통해 주증기 배관으로 전달되며, 이는 고압(HP, High-Pressure) 증기 터빈과 연결된다. nominal(정격) 조건에서의 superheater의 주증기 출구 조건은 538° C, 10 MPa이다.
그림 6(a)에는 시스템의 측면도가 개략적으로 표현되어 있다. 이 시스템은 여섯 번의 패스를 거치는 튜브 조립 구조(six–pass tube assembly configuration)로 구성되며, 증기는 그림의 오른쪽 상단에 위치한 입구 헤더를 통해 유입되어 왼쪽 상단에 위치한 출구 헤더를 통해 배출된다. 또한, 실제 시스템은 그림 6(b)에 도시된 정사영(orthographic) 도기에서 볼 수 있듯이 가로 방향으로 총 74개의 유동 회로(flow circuit)를 포함한다. 각 유동 회로는 그림 6(a)에 보이는 여섯 번의 패스를 거치는 튜브 조립체로 구성되며, 서로 엇갈리게 (staggered arrangement) 배치되어 있다.
이 시스템은 그림 6(a)에 표시된 위치에 설치된 열전대(thermocouple)를 통해 풍부한 온도 측정 데이터를 확보하고 있다. 전체 74개의 유동 회로 중 18개의 유동 회로에 열전대가 설치되어 있어, 일반적인 발전소의 superheater 시스템과 비교했을 때 매우 정밀하게 계측된 시스템이다. 이렇게 계측된 그림 6(a)에 나타난 다양한 위치에 설치되어 있으며, 두 가지 유형으로 분류된다.
첫 번째는 튜브 외경 벽면 온도를 측정하기 위한 열전대로, E6' , E49' , E75' , RB1, RB2로 표기되며 튜브 벽의 외부 표면에 용접되어 있다. 두 번째는 연소가스(flue gas) 온도를 측정하기 위한 열전대로, G47' , G71' 으로 표기되며, 튜브 벽에 직접 부착되지 않고 튜브 지지대 위에 얹혀 설치된다. 각 위치 태그에 포함된 숫자는 센서가 설치된 높이를 나타낸다.
이 시스템은 헤더 출구에서의 증기 온도를 평균하여 측정한 주증기 온도 값 또한 확보되어 있다. 추가적으로, 그림 6(a)에서 좌측의 연소가스 흐름 경로를 따라 위치한 유입 연소가스 온도도 발전소의 운전 데이터로부터 제공된다. 최종 superheater의 상류(left side HRSG upstream)에 위치한 4개의 열전대 세트를 이용하여 유입 연소가스 온도의 평균을 계산하고, 이는 하이브리드 모델의 입력 데이터로 사용된다.

4.2. 플랜트 B 최종 superheater(과열기) 시스템 (PC 보일러 발전소)

본 연구에서 분석된 두 번째 최종 superheater 시스템은 플랜트 B는 786 MW의 발전 용량을 갖는 PC–fired(분탄 연소) 발전소 보일러의 일부이다. 이 PC 보일러는 여섯 개의 분쇄기(pulverizer)를 통해 역청탄(bituminous coal)을 연소시키며, 정격 조건에서 주증기를 537° C, 27 MPa로 생산한다. 선택된 superheater 시스템의 구성은 그림 7에 나타나 있다.
이 시스템은 two–pass(2단 통과) 튜브 조립 구조로 구성된다. 시스템의 각 패스(pass)는 여섯 개의 개별 튜브로 이루어져 있으며, 이는 첫 번째 헤더에서 수직 방향으로 출구를 갖고, 180° 의 부드러운 곡선을 따라 다시 수직으로 연장되어 출구 헤더로 연결되는 형식이다. 참고로 그림 7와 개략도에서는 이러한 곡선 전이를 각진 형태로 표현하고 있으며, 이는 증기 입 · 출구 헤더에 연결된 부분이다.
그림 7에 나타난 바와 같이, 여섯 개의 개별 튜브는 오른쪽에서 왼쪽 방향으로 T1부터 T6까지 번호가 매겨져 있으며, T1이 가장 길고 T6가 가장 짧으며, 연소가스(flue gas)는 오른쪽에서 왼쪽 방향으로 수평 흐름을 가진다. 연소가스 흐름 경로상 T1은 첫 번째이자 마지막 튜브이고, T6는 가장 안쪽에 위치하여 연소가스 흐름에 가장 직접적으로 노출되는 튜브이다.
증기는 시스템의 오른쪽 상단에 위치한 입구 헤더를 통해 유입되며, 여섯 개의 곡선형 튜브로 균등하게 분배되어 수직 방향으로 하강하고, 왼쪽 상단에 위치한 출구 헤더를 통해 시스템을 빠져나간다. 이 출구 헤더는 주증기 배관과 연결되어 있으며, 이는 다시 HP(high–pressure) 증기 터빈으로 이어진다. 그림 7은 시스템의 측면도를 나타낸다.
전체 최종 superheater 시스템은 그림 7에 나타난 두 개의 패스를 가지는 여섯 개의 U자형 튜브로 구성된 동일한 유동 조립체(flow assembly) 197개로 구성되어 있으며, 이들은 서로 뒤에 쌓이는 형태로 배열되어 있다. 이 시스템 또한 비정상적으로 정밀하게 계측되어 있으며, 보일러의 폭 방향을 따라 선택된 조립체와 튜브–헤더 연결부에 장착된 열전대 75개가 penthouse(상부 밀폐 공간)에 설치되어 튜브의 온도를 측정할 수 있다.
그러나 이 시스템의 연소가스 유입 온도(그림 7의 오른쪽 측)는 발전소 histonian 시스템으로부터 제한된 시간 구간에 대해서만 제공되며, 모델 시뮬레이션에 필요한 전체 기간에 대해서는 제공되지 않았다. 따라서 제한된 데이터셋을 기반으로, 연소가스 유입 온도를 발전소 총 부하(MW)의 함수로 나타내는 2차(quadratic) 상관식을 개발하였으며, 이를 전체 데이터셋의 시뮬레이션에 활용하였다.
PC 보일러 시스템으로부터 얻은 superheater 데이터는 NGCC 발전소에서 얻은 데이터와 비교했을 때, 체계적(systematic) 및 무작위(random) 잡음 수준이 훨씬 더 높고, 공간 분포(spatial distribution) 도 더 복잡하여 분석에 더 큰 도전 과제를 제공함이 확인되었다.

present more challenges as compared to that obtained from NGCC plants in terms of significantly higher systematic and random noise and considerable spatial distribution.

4.3. Dynamic First-Principles (FP) superheater model

The dynamic first-principles superheater model used in the hybrid modeling framework is developed in our previous work [5]. The model used differential mass and energy balance equations for the flow streams along with consideration of metal tube wall temperature dynamics based on thin-walled assumptions. As illustrated in Fig. 8, the model consists of a control volume block approach. This provides a modular unit which can be combined in any form based on any industrial system geometry and configuration [82]. The approach can be easily extended to multiple superheaters/reheaters arranged in series /parallel.

In Fig. 8, a cross-flow arrangement is shown for the system with flue gas flow depicted by a green arrow flowing in the horizontal 'y' direction whereas steam flow is depicted by a blue arrow in the vertical 'z' direction. However, this considered flow pattern is generic and may be modified as per the system's specifics. Also, the model is developed with the assumption that property changes for both the flow streams occur in their respective flow directions only. Hence, no change in the thermo-physical properties is considered in the width direction as shown in Fig. 8 for the two streams in the developed model. The differential equations are solved for each stream only in their respective flow direction neglecting the other directions. The dominant heat transfer mechanism considered for the model is convection only without any radiative effects.

The modeling equations for both the steam and flue gas are as follows:

Mass Balance Equations:

$$\frac{\partial \rho_{st}}{\partial t} + \frac{\partial (\rho_{st} v_{st})}{\partial z} = 0 \quad (2)$$

$$\frac{\partial \rho_{fg}}{\partial t} + \frac{\partial (\rho_{fg} v_{fg})}{\partial y} = 0 \quad (3)$$

Energy Balance Equations:

$$\frac{\partial T_{st}}{\partial t} + v_{st}\frac{\partial T_{st}}{\partial z} = \frac{q_{wall,st}}{\rho_{st} c_{p,st}} \quad (4)$$

$$\frac{\partial T_{fg}}{\partial t} + v_{fg}\frac{\partial T_{fg}}{\partial y} = \frac{q_{wall,fg}}{\rho_{fg} c_{p,fg}} \quad (5)$$

In addition to the mass and energy balance equations for steam and flue gas flow, the dynamic energy balance across the metal tube wall assuming thin-walled tube is also considered for the superheater system using the equation:

$$m_{tube} C_{p,tube} \frac{dT_{tube}}{dt} = h_{conv,fg} A_o (T_{fg,in} - T_{tube}) - h_{conv,st} A_i (T_{tube} - T_{st,out}) \quad (6)$$

Furthermore, the heat transfer coefficients and other associated parameters considered for the model are calculated using rigorous property correlations for both the steam and flue gas side. The steam side heat transfer coefficient is calculated using Gnielinski correlation for smooth tubes. The flue gas side heat transfer coefficient is calculated using Gnielinski correlation for flow across tube bundles. Non-uniformity at the inlet to the superheater on the flue gas side is taken into consideration by accounting for void fraction and tube arrangement factor based on inline and staggered tube arrangement. The complete set of modeling equations for the same can be found in our previous publication [5].

The entire superheater systems for both Plant A and Plant B shown in Figs. 6 and 7, are divided into individual control volumes as shown in Fig. 8 and the modeling equations from Eqs. (2) to (6) are solved for each of these control volumes. Since the modeling equations were PDEs, the method of lines is used to convert these PDEs into ODEs. The reformulated ODEs are coupled with the algebraic equations making the entire system a DAE model. Fig. 9 shows the layout of both the superheater systems in control volumes and these entire systems have been solved in MATLAB using the DAE solver 'ode15s' [82].

3. Methodology for hybrid modeling of steam superheater system

This section discusses the various hybrid structures considered in this work by hybridizing the FP and AI models. For both superheater systems

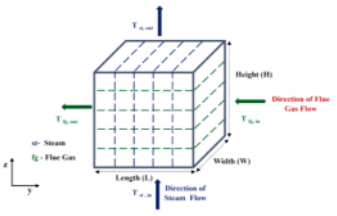

Fig. 8. Control volume block of the dynamic first principles superheater model.

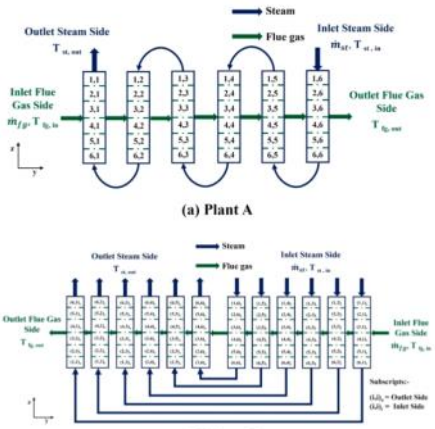

Fig. 9. Final superheater system layout using control volumes (second index of individual control volumes represents actual pass number of the superheater system) (a) Plant A and (b) Plant B.

(i.e., NGOC and coal-fired power plants) discussed in Section 4, the key process variables include the transient outlet temperature profiles of steam and flue gas, as well as the outer tube metal wall temperatures of superheater tubes. It should be noted that the steam from the superheater often directly goes to the steam turbine and therefore that temperature directly affects the power generation thus predictive modeling of the main steam temperature and its spatio-temporal variation are important for ensuring highly efficient operation of the power plant especially under load-following operation. Spatio-temporal distribution of tube wall temperature affects the thermal stress in the boiler and therefore tube life. Thus, a predictive model of these temperatures can be useful for eventually developing a monitoring tool. Exit flue gas temperature from the superheater and its spatio-temporal distribution are valuable for understanding heat transfer efficiency affected by plant operation, local variation in heat transfer resistance due to possible fouling, non-uniform distribution of flue gas flow especially under load-following and/or low load operation of the plant, etc. However, the selection of the optimal hybrid FP + AI structure (series, integrated or parallel) may not be obvious for transient modeling of these key performance variables in the superheaters. Fig. 10 shows the overall methodological workflow undertaken in this work.

In what follows the specific methodology used in this work for the final hybrid structure/model selection for a specific variable is described. As discussed in Section 3, among the different hybrid FP + AI model structures, one of the primary advantages of the parallel hybrid configuration is the flexibility to develop and simulate the associated FP and AI models separately and independently, thus leading to relatively faster computation for a given size of available data, compared to the series and integrated structures. Therefore, the parallel hybrid FP + AI model structure is considered as the baseline model for all variables undertaken in this work and then if its performance is not found to be acceptable, then other structures are investigated. While modeling the

4.3. 동적 First-Principles(FP, 물리 기반) superheater(과열기) 모델

하이브리드 모델링 프레임워크에 사용된 동적 first-principles superheater 모델은 선행 연구 [5]에서 개발되었다. 이 모델은 유동 스트림(flow stream)에 대한 질량 및 에너지 수지 미분방정식을 사용하며, 얇은 벽 가정(thin-walled assumptions)을 기반으로 한 금속 튜브 벽의 온도 동역학 또한 고려한다.

그림 8에 나타난 바와 같이, 이 모델은 제어 체적 블록(control volume block) 접근법으로 구성된다. 이러한 방식은 어떠한 산업 시스템의 형상 및 구성에도 기반하여 자유롭게 결합할 수 있는 모듈형 유닛을 제공한다[82]. 이 접근법은 일련 또는 병렬로 배열된 다수의 superheater/reheater(과열기/재열기)로도 손쉽게 확장 가능하다.

그림 8에서는 횡류(cross-flow) 배열의 시스템에 대해 나타나 있으며, 연소가스(flue gas)는 녹색 화살표로 수평 'y' 방향으로 흐르며, 증기(steam)는 파란 화살표로 수직 'z' 방향으로 흐른다. 그러나 이 유동 패턴은 일반적인 형태이며, 시스템의 특정 구성에 따라 수정될 수 있다. 또한, 이 모델은 두 유동 스트림 각각의 흐름 방향에 대해서만 물성(property)의 변화를 고려하도록 개발되었다. 즉, 그림 8에서 나타난 바와 같이, 너비 방향에서는 열역학적 물성의 변화가 고려되지 않는다. 미분방정식은 각각의 유동 스트림에 대해 그들의 흐름 방향에서만 풀리며, 다른 방향은 무시된다.

모델에서 고려되는 주요 열전달 메커니즘은 대류(convection)만 포함되며, 복사 효과(radiative effects)는 고려되지 않는다.

증기 및 연소가스(flue gas)에 대한 모델링 방정식은 다음과 같다:

질량 수지 방정식(Mass Balance Equations):

$$\partial \rho_{st}/\partial t + \partial (\rho_{st} \cdot v_{st})/\partial z = 0 \quad \text{(식 2)}$$

$$\partial \rho_{fg}/\partial t + \partial (\rho_{fg} \cdot v_{fg})/\partial y = 0 \quad \text{(식 3)}$$

에너지 수지 방정식(Energy Balance Equations):

$$\partial T_{st}/\partial t + v_{st}\,\partial T_{st}/\partial z = q_{wall,st} / (\rho_{st} \cdot c_{p,st}) \quad \text{(식 4)}$$

$$\partial T_{fg}/\partial t + v_{fg}\,\partial T_{fg}/\partial y = q_{wall,fg} / (\rho_{fg} \cdot c_{p,fg}) \quad \text{(식 5)}$$

증기 및 연소가스(flue gas) 흐름에 대한 질량 및 에너지 수지 방정식 외에도, 얇은 벽 가정(thin-walled assumption)을 기반으로 한 금속 튜브 벽을 가로지르는 동적 에너지 수지 또한 superheater 시스템에 대해 고려되며, 이는 다음과 같은 식으로 표현된다:

$$m_{tube} \cdot C_{p,tube} \cdot dT_{tube}/dt = h_{conv,fg} \cdot A_o \cdot (T_{fg,in} - T_{tube}) - h_{conv,st} \cdot A_i \cdot (T_{tube} - T_{st,out}) \quad \text{(식 6)}$$

또한, 모델에서 고려되는 열전달 계수(heat transfer coefficient) 및 기타 관련 매개변수들은 증기 및 연소가스 측 모두에 대해 엄밀한 물성 상관식(property correlation)을 통해 계산된다. 증기 측의 열전달 계수는 매끄러운 튜브에 대한 Gnielinski 상관식을 사용하여 계산된다. 연소가스 측에서 superheater 입구에서의 비균일성은 공극률(void fraction)과 튜브 배열 인자(tube arrangement factor)를 고려하여 반영되며, 이는 정렬형(inline) 및 엇갈림형(staggered) 튜브 배열에 기반한다. 이에 대한 전체 모델의 방정식 세트는 선행 논문 [5]에 수록되어 있다.

Plant A와 Plant B의 전체 superheater 시스템(그림 6 및 7 참조)은 그림 8에 나타난 바와 같이 개별 제어 체적(control volume)으로 분할되며, 식 (2)부터 (6)까지의 모델링 방정식이 각 제어 체적마다 해석된다. 이러한 모델링 방정식은 편미분방정식(PDE)이므로, 선형화 방법(method of lines)을 통해 이 PDE들을 상미분방정식(ODE)으로 변환한다. 재구성된 ODE는 대수방정식(algebraic equation)과 결합되어 전체 시스템은 DAE(미분–대수 방정식) 모델이 된다.

그림 9는 제어 체적 단위로 나뉜 두 superheater 시스템의 구성을 보여주며, 전체 시스템은 MATLAB의 DAE 해석기 'ode15s' [82]를 사용하여 해석되었다.

5. Methodology for hybrid modeling of steam superheater system

이 절에서는 FP(First-Principles, 물리 기반) 모델과 AI 모델을 하이브리드화하여 고려한 다양한 하이브리드 구조에 대해 설명한다. 4장에서 다룬 두 superheater 시스템(즉, NGCC와 석탄 화력발전소) 모두에 대해 주요 공정 변수는 다음과 같다:

- 증기 및 연소가스의 출구 온도 변화 프로파일 (transient outlet temperature profiles)
- superheater 튜브의 외부 금속 벽 온도 (tube metal wall temperatures)

그러나 superheater 내 주요 성능 변수들의 과도 상태(transient) 모델링에 대해 최적의 하이브리드 FP + AI 구조(직렬, 통합 또는 병렬)를 선택하는 것은 명확하지 않을 수 있다. 본 연구에서 수행된 전체 방법론적 워크플로우는 그림 10에 제시되어 있다.

이후에서는 특정 변수에 대한 최종 하이브리드 구조/모델 선택에 사용된 구체적인 방법론을 설명한다. 3장에서 논의한 바와 같이, 다양한 하이브리드 FP + AI 모델 구조 중 병렬(parallel) 하이브리드 구성의 주요 장점 중 하나는 FP 모델과 AI 모델을 각각 독립적으로 개발 및 시뮬레이션할 수 있다는 유연성이다. 이로 인해 주어진 데이터 크기에 대해 직렬(series) 및 통합(integrated) 구조에 비해 상대적으로 더 빠른 연산이 가능하다. 따라서 본 연구에서는 모든 변수에 대해 병렬 하이브리드 FP + AI 모델 구조를 기준(baseline) 모델로 고려하고, 그 성능이 만족스럽지 않을 경우에만 다른 구조들을 추가로 검토한다.

Plant A와 superheater 시스템에 대해 증기, 연소가스, 그리고 튜브 벽의 과도 온도 프로파일(transient temperature profiles)을 모델링하는 과정에서, 병렬 하이브리드 모델은 MAE(mean absolute instantaneous error) 값이 기준 상한인 10° C를 초과하는 좁 편저히 높은 수준으로 나타남을 확인하였다.

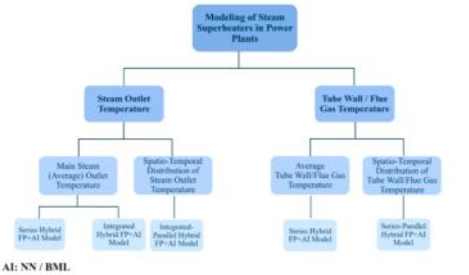

Fig. 10. Overall methodological flowchart showing different configurations of hybrid models used for representing the key performance variables in the superheaters.

transient temperature profiles of steam, flue gas, and tube wall for the superheater system at Plant A, it is observed that the parallel hybrid model leads to significantly higher MAIE values exceeding the desired upper bound of 10 °C. On the contrary, when the intermediate predictions from the FP model for all operational process variables are included as additional synthetic inputs for the AI models during training, thus leading to the development of the series hybrid FP + AI structure, the prediction accuracies of the resulting hybrid models improve significantly. Thus, in this work, the series hybrid FP + AI model has been considered as the optimal hybrid model for representing the average temperature profiles of main steam, flue gas, and outer tube wall of the superheater system at Plant A. However, during modeling the main steam outlet temperature profile for the superheater system at Plant B, it is observed that both the parallel and series hybrid FP + AI models lead to much inferior predictive capabilities especially during validation. The relatively inaccurate prediction of the transient steam temperature profile using dynamic data-driven residual models may possibly stem from the lack of data richness as well as the high uncertainties generally associated with coal-fired plants due to ash deposits and flow maldistribution. In such cases, it may be desired that information is internally exchanged between the FP and AI models through an integrated configuration to address the parametric uncertainties present in the standalone FP model and hence, eventually improve the predictive performance of the hybrid model. This approach also conserves the energy balance since the final output is from the FP model.

The optimal series and integrated hybrid FP + AI structures obtained for modeling the average temperature profiles of the respective process variables in the superheater systems at Plants A and B respectively can further be coupled with a second AI model in parallel to account for the spatio-temporal distribution of the same variables across different locations within the superheaters. It is to be noted that the parallel hybrid structures allow the development of the individual FP and AI models independently without requiring sequential information exchange, thus leading to faster computation during simulation. The parallel hybrid models are found to yield best results for modeling the spatio-temporal distribution of tube wall, flue gas and steam temperatures at different locations within the superheaters at Plants A and B, thus leading to the development of series–parallel and integrated-parallel hybrid FP + AI models, respectively.

The specific types of AI model involved in the hybrid FP + AI configurations also play an important role in determining the choice of the optimal hybrid model. While all implementations of hybrid models presented in this work consider the use of both FP + NN and FP + BML structures for representing all three process variables, a specific type of data-driven model can be chosen, if needed, based on a specific objective to be satisfied and the inherent advantages and disadvantages of various candidate AI-based modeling approaches. For instance, if it is desired to accurately represent a process variable with fast transients resulting in highly nonlinear dynamic temperature profiles, the hybrid FP + NN model may be preferred over FP + BML. On the contrary, the hybrid FP + BML models are found to result in a significantly superior predictive performance for the operational variables that are likely to be corrupted with uncertainties including colored noise while also enhancing model interpretability and sparsity, albeit leading to a much higher computational expense as compared to the FP + NN model. Furthermore, it is to be noted that for all results discussed in this paper which have been obtained from the optimal FP + NN model, the associated NN model corresponds to the most optimal all-nonlinear static-dynamic NN structure among NLZ-NLD, NLD-NLd, and NLd || NLD models (as discussed in Section 2.2) in terms of predictive accuracy and computational expense for the respective training data. However, the authors would like to mention that it is neither desirable nor realistic to conclude the superiority of a particular type of AI model over another since the relative performance of data-driven models does depend on several factors [81] including nonlinearity and transient characteristics of the data, transient error in the output from the FP model, etc. Thus, the specific hybrid structure that is found to work the best for representing a variable in this work is not necessarily unique, neither does it indicate

반대로, 모든 온전 공정 변수에 대해 FP 모델에서 생성된 중간 예측값(intermediate predictions)을 AI 모델의 학습 시 추가적인 합성 입력(synthetic inputs)으로 포함시키는 방식으로 직렬 하이브리드(series hybrid) FP + AI 구조를 개발한 경우, 결과 하이브리드 모델의 예측 정확도가 크게 향상되는 것으로 나타났다. 따라서 본 연구에서는 Plant A의 superheater 시스템에서 주 증기, 연소가스 및 외부 튜브 벽의 평균 온도 프로파일을 나타내는 데 있어 직렬 하이브리드 FP + AI 모델을 최적의 하이브리드 모델로 간주하였다.

그러나 Plant B의 superheater 시스템에 대해 주 증기 출구 온도 프로파일을 모델링하는 과정에서는 병렬 및 직렬 하이브리드 FP + AI 모델 모두 특히 검증 단계에서 예측 성능이 매우 떨어지는 것으로 나타났다. 동적 데이터 기반 잔차 모델(dynamic data–driven residual model)을 이용한 과도 증기 온도 프로파일의 상대적으로 부정확한 예측은, 데이터의 풍부함 부족이나 석탄 화력발전소 특유의 높은 불확실성에 (재(ash) 침적, 유동 불균일성 등)에서 기인할 수 있다. 이러한 경우, 독립형 FP 모델의 파라미터 불확실성을 해결하기 위해 FP 모델과 AI 모델 간에 내부적으로 정보를 교환하는 통합형(integrated) 구성이 필요할 수 있으며, 이는 궁극적으로 하이브리드 모델의 예측 성능을 향상시키는 데 기여한다. 또한 이 접근법은 최종 출력이 FP 모델로부터 나오므로 에너지 수지를 보존하는 장점도 있다.

Plant A와 B의 superheater 시스템에서 각각의 공정 변수 평균 온도 프로파일을 모델링하는 데 최적의 직렬 및 통합 하이브리드 FP + AI 구조가 도출되었으며, 이는 이후 superheater 내 다양한 위치에 걸친 동일 변수의 시공간 분포(spatio–temporal distribution)를 설명하기 위해 병렬로 두 번째 AI 모델과 결합될 수 있다. 주목할 점은, 병렬 하이브리드 구조는 FP 모델과 AI 모델 각각을 독립적으로 개발할 수 있게 하여 순차적인 정보 교환이 필요하지 않으며, 시뮬레이션 시 더 빠른 연산이 가능하다는 점이다.

Plant A 및 B의 superheater 내 다양한 위치에서 튜브 벽, 연소가스 및 증기 온도의 시공간 분포를 모델링하는 데 있어 병렬 하이브리드 모델이 가장 우수한 결과를 보였으며, 그에 따라 직렬–병렬(series–parallel) 및 통합–병렬(integrated–parallel) 하이브리드 FP + AI 모델이 각각 개발되었다.

하이브리드 FP + AI 구성에서 사용되는 AI 모델의 구체적인 유형 또한 최적 하이브리드 모델 선택에 중요한 역할을 한다. 본 연구에서 제시된 모든 하이브리드 모델 구현은 세 가지 공정 변수를 모두 표현하기 위해 FP + NN(Neural Network) 및 FP + BML(Bayesian Machine Learning) 구조의 사용을 고려하고 있으나, 특정 목적을 만족시키기 위해 필요시 특정 유형의 데이터 기반 모델을 선택할 수 있으며, 이는 다양한 AI 기반 모델링 접근 방식의 고유한 장단점에 따라 결정된다.

예를 들어, 빠른 과도(transient)를 가지며 고도로 비선형적인 동적 온도 프로파일(dynamic temperature profiles)을 정밀하게 표현하고자 할 경우, 하이브리드 FP + NN 모델이 FP + BML 모델보다 선호될 수 있다. 반대로, 컬러 잡음(colored noise) 등 불확실성에 의해 오염될 가능성이 높은 온전 변수들에 대해서는 하이브리드 FP + BML 모델이 훨씬 뛰어난 예측 성능을 제공하는 것으로 나타났으며, 동시에 모델 해석 가능성(model interpretability) 및 희소성(sparsity) 또한 향상된다. 다만 이러한 이점은 FP + NN 모델에 비해 훨씬 더 높은 계산 비용을 초래한다는 단점도 있다.

또한 본 논문에서 논의된 모든 결과 중 최적 FP + NN 모델로부터 도출된 결과에 사용된 NN 모델은 Section 2.2에서 논의된 바와 같이, 주어진 학습 데이터에 대해 예측 정확도 및 계산 비용 측면에서 가장 우수한 전부 비선형 정적–동적 NN 구조(all–nonlinear static–dynamic NN structure)에 해당하며, 이는 NLS–NLD, NLD–NLS, NLS || NLD 구조 중 하나이다.

그러나 저자들은 특정 유형의 AI 모델이 다른 모델보다 우월하다고 결론짓는 것은 바람직하지도, 현실적이지도 않다고 명시한다. 데이터 기반 모델의 상대적인 성능은 데이터의 비선형성 및 과도 특성, FP 모델의 출력에서 발생하는 과도 오차 등 여러 요인 [81] 에 따라 달라지기 때문이다. 따라서 본 연구에서 특정 변수를 표현하는 데 가장 효과적인 것으로 나타난 하이브리드 구조가 유일하거나, 다른 발전소의 데이터에서도 유사한 결과가 도출된다고 일반화할 수는 없다.

that similar observations would be made for data from another plant.

6. Results and discussion

The performance of the different hybrid models formed by the synergistic integration of the standalone FP model with both types of AI models as discussed in Section 3 are evaluated by implementing them to improve model performance for critical variables such as main steam temperature for the two industrial final steam superheater systems described in Section 4. For all case studies, the input and output variables of the data-driven models are normalized, and approximately 60 % of the total dynamic data are used to train the corresponding AI (and hence, FP + AI) models. Cross validation is performed for both case studies using the k-fold method (with k = 5). For all structures and approaches the performances of different candidate models have been compared in terms of RMSE calculated between the measured output data $\left(y_{r,meas}(t)\right)$ and model predictions $\left(y_{r,mod}(t)\right)$, defined as:

$$\mathrm{RMSE}_r = \sqrt{\frac{1}{t_e}\left(y_{r,meas}(t) - y_{r,mod}(t)\right)^2} \tag{7}$$

where, t_e denotes the number of time steps under consideration. Furthermore, for developing accurate models of dynamic processes, especially energy systems, one of the key performance metrics is the instantaneous error [823] between actual measurements and model predictions. This measure does not get appropriately captured by RMSE or other similar measures. High instantaneous errors are unacceptable for a broad range of process applications, such as process monitoring, control, and dynamic optimization, that would utilize instantaneous predictions for decision-making. Therefore, significantly higher values of instantaneous error can eventually lead to various undesirable situations such as unsafe operation, equipment failure, poor product quality, and so on. For a measure of instantaneous error, in addition to RMSE, the MAIE is also calculated to compare prediction performances of the hybrid FP + AI models at any given instance. The MAIE for the i^{th} output variable is defined as:

$$\mathrm{MAIE}_r = \max\left\{\left|y_{r,meas}(t) - y_{r,mod}(t)\right|\right\}$$
$$\forall t \in \{1, 2, \cdots, t_e\} \tag{8}$$

While results from the hybrid FP + AI models have been compared with the entire time-series temperature measurements that are available for the main steam, outer tube wall, and flue gas at different locations for both the superheater systems, only a subset of those results is included in this paper for brevity. Furthermore, all comparisons regarding the relative computational expense discussed in this paper correspond to that involved during training of the optimal data-driven models in the hybrid structures. During simulation, i.e., using the optimal hybrid FP + AI models for future time-series predictions, the AI models generate the respective output variables almost instantaneously. Thus, the simulation times associated with the hybrid FP + AI models depend mostly on the time the FP model takes to simulate through a single time step. In particular, the predictive capabilities of the proposed hybrid FP + AI models have been evaluated based on various performance metrics obtained while predicting the transient temperature profiles of the process variables of interest, i.e., the outlet steam, tube wall, and flue gas temperatures.

6.1. Modeling of steam outlet temperature

The proposed hybrid models demonstrate sufficient flexibilities for not only predicting the main steam outlet temperatures of both power

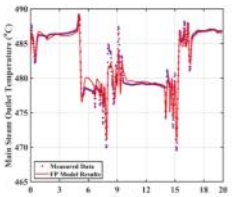

Fig. 11. Comparison of results from the standalone FP model with measured data for the main steam outlet temperature for Plant A.

plant systems under consideration, but also modeling the spatio-temporal variation of the steam outlet temperatures along the width direction of the superheaters (refer Fig. 6 (b)). However, it is worth noting that the specific type of hybrid model that can be implemented for modeling a particular variable of interest may vary based on the specific objective to be addressed within the system as well as the limitations associated with one or more hybrid structures considered in this paper.

6.1.1. Results for the main steam outlet temperature ($T_{w,out}$)

Prediction of the main steam outlet temperature in power plant systems within sufficient accuracy is crucial for both profitability and efficiency aspects, as well as for preventing damage of the steam turbine [803]. It is to be noted that the main steam outlet temperature is a controlled variable, and measured. A predictive model of the main steam temperature can also help plant operation to ensure that instantaneous variation and overall deviation from the desired value remain acceptable. In addition to the main steam outlet temperature, this work also focuses on the development of predictive model(s) for additional transient temperature profiles, especially at locations where measurements are not available.

- *Results from the Series Hybrid FP + AI Models (Plant A)*

The simulation and validation of the FP model with respect to the final superheater system at Plant A is performed using the control volume discretization scheme and available plant input operating data, as shown in Fig. 9 (a), for a continuous span of around 20 h. The input profiles of all the variables taken from the operating industrial data have been shown in Fig. A. 1 in Appendix A. It is observed from Fig. A. 1, that the selected dataset has sufficient variabilities in between successive steady state zones. Overall, the data contains three steady zones in the entire 20 h duration between 0–3 h, 11–14 h and 17–20 h providing a rich source of data for simulating the load-following operations of the system.

The validation results of the standalone FP model for the main steam outlet temperature is shown in Fig. 11. In Fig. 11, the series, "Measured Data", represents the actual industrial operating data obtained from the

Table 1
List of model input and output variables in the series hybrid FP + AI models for the superheater system of Plant A.

Variables used in Fig. 2	Actual input/output variables for the series hybrid FP + AI model in terms of process variables for Plant A
$u(t)$	$T_{s,in}, \dot{m}_s, T_{fg,in}, \dot{m}_{fg}$
$y_{FP}(t)$	[illegible]
$u_{AI}(t)$	–
$y_{pred}(t)$	[illegible]

Table 2
Comparison among FP, FP + NN, and FP + BML models in terms of RMSE, MAIE, number of parameters and computational time for training the main steam outlet temperature for Plant A.

Types of Model	Number of Model Parameters	Training Computational Time for respective AI models	Main Steam Outlet Temperature (°C)	
			RMSE	MAIE
FP	–	–	1.0	3.6
FP + NN	182	2.3 min	0.2	1.8
FP + BML	136	21.7 h	0.8	3.9

plant historian and the series, "FP Model Results", represents the results obtained by simulating the standalone dynamic FP model (refer Section 4.3) for Plant A in absence of any data-driven augmentation. As shown in Fig. 11, the performance of the FP model has been validated for predicting the main steam outlet temperature ($T_{s,out}$, refer Fig. 9) by comparing the measured data (purple dots) with the FP model results (red line). It can clearly be observed from Fig. 11 that although the FP model trends well with the measured data in the steady-state zones noted above, the FP model predictions show some deviations with respect to the measurements during dynamic operations, especially during 6–10 h and 14–18 h. Overall, the standalone FP model yields an RMSE of 1.0 °C and a MAIE of 3.6 °C for the entire duration.

The application of the series hybrid FP + AI model structure (refer Fig. 2) to Plant A provides updated results for the main steam outlet temperature ($T_{s,out}$, refer Fig. 9). The input/output variables as shown in Fig. 2 corresponding to the model/process variables for the superheater system in Plant A have been listed in Table 1, where $y_{pred}(t)$ signifies the corrected output variables obtained after passing the outputs from the FP model, i.e., $y_{FP}(t)$ through the data-driven model. The series hybrid FP + AI model follows a sequential approach where information flows in a single direction, i.e., from the FP to the AI models.

In Table 1, out of the eight output variables obtained for Plant A considering the specific implementation of the series hybrid model, while all may be useful to know for proper unit operation, the accurate prediction of the main steam outlet temperature is critical since it not only impacts plant operation but also directly impacts turbine and tube life [64]. The validation results of the series hybrid models for the main steam outlet temperature are shown in Fig. 12. As shown in Fig. 11, the standalone FP model has some deviations while predicting the main steam outlet temperature with respect to the measured data, resulting in an approximate RMSE of 1.0 °C. The black dotted vertical lines in Fig. 12 signify the total duration of dynamic time-series data (3–15 h) used for training both AI (and hence, FP + AI) models. It can be observed that the hybrid FP + NN and FP + BML models show improvement in predictive capabilities over the standalone FP model not only for the dynamic data used for training the respective AI models, but also for the validation data. It is to be mentioned here that the all-nonlinear parallel (NLS || NLD) static-dynamic NN model (as shown in Fig. 1 (c)) has been chosen to represent the NN model in the hybrid FP + NN structure, due to its relative superiority among the other two candidate architectures. The RMSE values in the prediction of the main steam outlet temperature, for instance, have been reduced from 1.0 °C, with respect to the standalone FP model, to 0.2 °C and 0.8 °C, for the hybrid FP + NN and FP + BML models, respectively. The comparison among the standalone FP and both types of hybrid models in terms of RMSE and MAIE, and the overall computational time for training the hybrid FP + AI models, have been shown in Table 2.

Fig. 13 shows a zoomed section (15–20 h) of the validation data shown in Fig. 12 for comparing the performances of the two AI models for the prediction of the main steam outlet temperature. It can be observed from Fig. 13 (b) that the FP + BML model shows a relatively larger mismatch with the measurements, and leads to much higher instantaneous errors as compared to the FP + NN model as shown in Fig. 13 (a) and Table 2. One of the primary reasons for such mismatch observed for the hybrid FP + BML model probably stems from the type

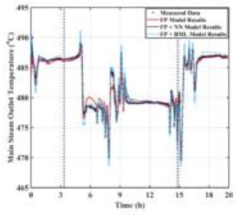

Fig. 12. Comparison of results among standalone FP, FP + NN and FP + BML series models with the measured data for the main steam outlet temperature for Plant A.

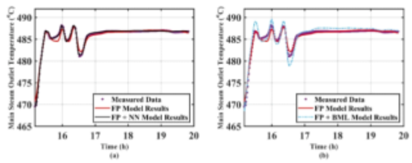

Fig. 13. Comparison of results among standalone FP and hybrid (a) FP + NN and (b) FP + BML models with the measured data for the main steam outlet temperature of Plant A.

of candidate basis functions considered during optimal model synthesis, in contrast to the activation functions used in the optimal NN model. While all standard NN activation functions are strictly bounded, the BML (i.e., BIDGAM) algorithm also considers unbounded candidate basis functions such as quadratic and bilinear combinations of input/output variables, thus leading to higher instantaneous errors while modeling highly complex dynamic data. Furthermore, the consideration of two different types of AI models in the hybrid framework also shows the tradeoff between prediction accuracy and computational expense involved during optimal model development (training). While the consideration of BML approaches in the hybrid series FP + AI structure yields a relatively lesser number of model parameters to be estimated during training, on the contrary, the FP + NN type of hybrid model is associated with a significantly lesser (faster) training computational time and superior predictive capabilities.

The complete list of all optimal candidate basis functions estimated for this case study by the BML algorithms, as well as their applicability to model/process variables, is provided in Tables A1 and A2 in Appendix A. From the list of selected candidate basis functions obtained from the optimal interpretable BML models as presented in these tables, it is evident that the consideration of $y_{FP}(t)$ as additional synthetic inputs for the AI models in the series architecture has a significant impact on the predictive performance of the resulting hybrid models, as compared to the parallel hybrid FP + AI structure discussed in Section 3.3. Furthermore, on implementation of the parallel hybrid FP + AI models (refer Section 3.3) for predicting $T_{s,out}$, it is observed that the resulting optimal models leads to MAIE values as high as around 16 °C which exceeds the acceptable limits considered in this work. It is worth mentioning that the transient temperature profiles observed for the NGCC power plant show relatively lesser uncertainties and hence improved/sufficient richness in measured data, as compared to the PC power plant. Therefore, the results obtained from the series hybrid model in this case are considered satisfactory for accurately predicting the main steam outlet temperature.

- *Results from the Integrated Hybrid FP + AI Models (Plant B)*

The final superheater system of Plant B (PC-fired boiler, refer Fig. 7) has been simulated and validated using similar methodology described for Plant A. The control volume discretization scheme of Plant B is shown in Fig. 9 (b), and like Plant A, inlet flowrates and temperatures of steam and flue gas obtained from plant operational data are considered as inputs to the standalone FP model. However, for this system, only the steam side input data, i.e., the steam inlet temperature ($T_{s,in}$) and steam mass flowrate ($\dot{m}_s$) are directly measured. The flue gas inlet temperature is calculated using a quadratic correlation for $T_{fg,in}$ (refer Eq. (B1)) relating flue gas inlet temperature with gross plant load (MW) for the entire dataset. Similarly, the flue gas inlet mass flowrate ($\dot{m}_{fg}$) is also not available from plant data and has been calculated from combustion calculations using coal flowrates, air flowrates and coal ultimate analysis data obtained from the plant. Fig. B1 in Appendix B shows the profiles of all input variables used in the simulation of Plant B for a continuous period of 27 days. The selected dataset shows significant changes in unit operation with frequent load changes between minimum, intermediate, and maximum load with sufficient dynamic and steady zones captured in the dataset. The load profile of Plant B (refer Fig. B2) for the entire 27 days simulation period can be found in Appendix B. Fig. B3 in Appendix B shows the performance of the standalone FP model for predicting the main steam outlet temperature with respect to the measured data available from the plant historian for a continuous operation of 27 days. While the FP model generally captures the trend in the system dynamics, its predictions remain consistently biased to the measured plant data with an overall RMSE of 19.5 °C and a MAIE of around 35 °C. Both the RMSE and MAIE values obtained from the standalone FP model violate the desirable limits considered in this work. The overprediction by the FP model as reflected especially by the high MAIE value can be attributed to the model predicting higher heat transfer than observed in the actual system. The reason for this high heat transfer prediction by the model could possibly be due to certain modeling assumptions considered for the standalone FP model development impacting the accuracy of the FP model results such as considering convection as the dominant heat transfer mechanism ignoring the radiative heat transfer between flue gas and outer tube surface. Also, only the temperature dependence of specific heat capacity ($c_{p,s}$, refer Eq. (4)) for steam side is considered in the model development and not the pressure dependence along the steam flow path.

It has been observed that the series hybrid FP + AI model (as discussed in Section 3.1) in this case (Plant B) yields satisfactory performance for the training data. However, the resulting optimal series hybrid model showed significantly higher mismatches and inferior predictive capabilities during simulation, leading to MAIE values as high as 21 °C for $T_{s,out}$ and therefore not acceptable. Modeling such energy systems can benefit from synergistic cross-coupling between the FP and AI models (i.e., integrated model as shown in Fig. 3). In the integrated hybrid model, the flue gas side heat flux $\left(q_{fg}\right)$, given by Eq. (9), has been modified in the formulation of the FP model to account for the uncertainties in the heat transfer rate by incorporating an additive correction term for the heat transfer coefficient ($h_{corr,fg}$), as defined in Eq. (10). In Eq. (10), $h_{conv,fg}$ refers to the original heat transfer coefficient calculated from the heat transfer correlations involved in the FP model,

참고 논문 페이지 8

and $T_{fg,in}$ and T_{tube} represent the inlet flue gas temperature and the outside tube wall temperature respectively.

$$q_0 = h_{corr,fg}\left(T_{fg,in} - T_{tube}\right) \tag{9}$$

$$q_0 = h_{corr,fg}\left(T_{fg,in} - T_{tube}\right) + h_{corr,fg}\left(T_{fg,in} - T_{tube}\right) \tag{10}$$

The corrective heat transfer coefficient ($h_{corr,fg}$) values are represented by the AI models (refer Fig. 5 (a)). A continuous duration spanning around 27 days of plant operational data has been considered, out of which only 9 days (concatenating windows spanning for 24 h continuous time series data measured every minute, leading to approximately 33 % of the total data) are chosen randomly. For these data, a single parameter constrained optimization problem given by Eq. (11) is solved by using a second-order constrained optimization approach. The squared error between the results from the FP model, i.e., $T_{st,out}$ (refer Fig. 9 (b)), and the respective plant measurements is minimized by optimizing $h_{corr,fg}$.

$$\min_{h_{corr,fg}} \left(T_{st,out,meas}(t) - T_{st,out,FP}(t)\right)^2$$

$$s.t. T_{st,out,FP} = f_{FP}\left(x, u, \theta_{FP}, h_{corr,fg}, t\right) \tag{11}$$

where, x denotes the state variables considered in the FP model and $f_{FP}(\bullet)$ denotes the system of FP model equations. The corrective term for the heat transfer coefficient ($h_{corr,fg}$) is expressed as a function of the input boundary conditions (i.e., $T_{st,in}$, $\dot{m}_{st}$, $T_{fg,in}$, $\dot{m}_{fg}$, please see Fig. B1) as model inputs. In addition to these four inputs, the attemperator spray flowrate $\left(\dot{m}_{spray}\right)$, as well as the valve openings on four inlet pipes connecting to the steam inlet header $(v_{p,1}, v_{p,2}, v_{p,C}, v_{p,D})$, are considered as additional inputs for the AI models. The list of the input/output variables considered for the integrated hybrid FP + AI model can be found in Table B1 in Appendix B. It should be noted here that out of the five additional inputs considered for the AI models only four input which are the valve openings $(v_{p,1}, v_{p,2}, v_{p,C}, v_{p,D})$ are directly measured in the plant using instruments. The attemperator spray flowrate $\left(\dot{m}_{spray}\right)$, although available from plant operating data is not a measured value and is calculated using a developed correlation by the plant based on valve openings and plant load.

The respective temporal variations of these additional input variables have been shown in Figs. B4 and B5 in Appendix B. It should be noted that, the improved estimate of the heat transfer coefficient is also expected to improve the predictions of the other variables of interest such as tube wall temperature and flue gas temperature, that are important variables for performance analysis, yet remains largely unmeasured in many power plants.

Fig. 14 shows the comparison between the integrated hybrid FP + NN and FP + BML models for the main steam outlet temperature in Plant B. It can be observed that the integrated hybrid FP + AI models accurately capture the overshoots and undershoots in the temporal profile of the main steam outlet temperature with desired accuracies.

The comparison among the different performance measures among the standalone FP, FP + NN, and FP + BML models has been provided in Table 3. Both types of hybrid FP + AI models significantly improve the prediction accuracy within the acceptable limits of RMSE and MAIE considered in this work, as can be seen in Table 3. It should be noted that the training computational times reported in Table 3 does not include the computational expense associated while generating the training data for the AI models by solving the constrained optimization problem. The training and prediction results obtained from the NN and BML models for $h_{corr,fg}$ have been shown in Figs. B6 and B7 in Appendix B. It should be noted that the negative values of the optimal $h_{corr,fg}$ corrects the over-prediction of the flue gas side heat transfer coefficient by the standalone FP model.

From Table 3, it is evident that both hybrid integrated FP + AI models show similar predictive performance for the main steam outlet temperature. However, the BML model requires less than one-third of the number of parameters used in the NN model. It is to be mentioned here that for all case studies, consistently higher computational expense associated with the training of the BML model can be attributed to the rigorous search for the globally optimal subset of well-defined basis functions using the branch and bound approach in the BIDEAM algorithm [7]. In addition to this, the approach explicitly accounts for noise that may be present in the training data as it simultaneously carries out uncertainty quantification alongside model parameter estimation. Furthermore, the mathematical model forms of the optimal parametric NN and BML models obtained for the estimation of $h_{corr,fg}$ have been included in Table B2 in Appendix B.

6.1.2. Results for the Spatio-Temporal distribution of steam outlet temperature

- *Results from the Integrated Parallel Hybrid FP + AI Model (Plant B)*

As discussed in Section 4.2, the final superheater system for Plant B under consideration consists of tubular flow circuits stacked one behind another across the heat transfer space. In the actual system configuration, there are 197 flow circuits in Plant B. However, constructing an accurate first-principles model for each flow circuit (location) along the width direction (refer Fig. 8) for the given system can be computationally impractical for most cases. Fig. C1 in Appendix C shows the temperature distribution in the width direction for the measured data of the steam outlet temperature for Plant B. It is to be mentioned that the legend "Average Measured Data" for the steam outlet temperature, as represented in Fig. C1 refers to the measured main steam outlet temperature available directly from plant historian. Additionally, in all the results shown for the integrated parallel hybrid model in Fig. C1 and Fig. 15, the legends "Max Measured Data" refers to the maximum value (in terms of absolute magnitude) observed and "Min Measured Data" refers to the minimum value (in terms of absolute magnitude) observed for any particular variable among the actual operating data.

Fig. C1 shows the temperature distribution for the measured data of the steam outlet temperature available from the industrial partner power plant for a continuous operational period of 27 days. In Fig. C1, the average measured data (purple dots) are shown, along with the maximum measured data (brown dots) and minimum measured data (cyan dots) representing the wide range of temperature distribution for the steam outlet temperature along the width direction for the superheater in Plant B. In Fig. C1,only two datasets for dynamic temperature profiles (termed as 'Loc 1' and 'Loc 2') corresponding to the maximum and minimum deviation from the average measured value, i.e., the steam outlet temperature respectively, have been considered. The standalone FP models developed for both the superheater systems (Plants A and B, refer Section 4.3) neglects variability of transport variables in the width direction. Inclusion of another dimension, i.e., the width direction may lead to excessive computational expense and hence, can be difficult for online adaptation. However, accurately predicting the temperature profiles at each tube assembly/location in the width direction will be useful for developing a health monitoring framework for the boiler components for damage prediction in each tube and predict potential tube failures in future. Therefore, such limitations present in a standalone FP model can be compensated with appropriate data-driven models. For such limitations in the FP model, a parallel hybrid configuration of FP and AI models may be beneficial.

In Plant B, the integrated hybrid approach where the AI model is used to represent the correction factor for the heat transfer coefficient is coupled with another AI model in parallel, thus yielding the integrated parallel hybrid FP + AI model. The integrated parallel model developed is then implemented for modeling the dynamic temperature profiles

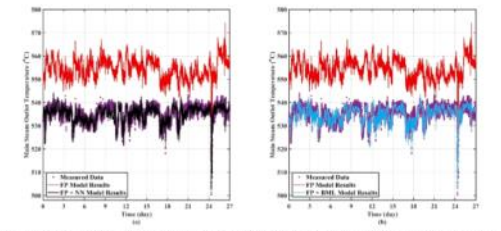

Fig. 14. Comparison of results between standalone FP vs hybrid (a) FP + NN and (b) FP + BML models for main steam outlet temperature with respect to the superheater system at Plant B.

Table 3
Comparison between hybrid integrated FP + NN and FP + BML models in terms of overall prediction RMSE, MAIE, number of parameter and training computational time for the main steam outlet temperature of Plant B.

Types of Models	RMSE (°C)	MAIE (°C)	Number of Model Parameters	Training Computational Time for the respective AI models
FP + NN	1.8	6.3	180	1.7 min
FP + BML	2.0	8.9	27	22.9 min

along the width direction of the superheater system in Plants B. Similar to the series hybrid FP + AI model (refer Eq. (13)), depending on the specific type of parallel hybrid structure, the target dynamic outputs of the second AI models is given by Eq. (12):

$$\Delta_y(t) = y_{j,meas}(t) - \hat{y}_{j,FP|AI_{corr}}(t) \tag{12}$$

where, Δ_y denotes the deviations, $y_{j,meas}(t)$ denotes the measured dynamic temperatures at all j tube assemblies/flow circuits along the width direction, and $\hat{y}_{j,FP|AI_{corr}}(t)$ denotes each of the respective (integrated) model predicted values of the average temperatures of the j^{th} output variable (refer Fig. 9).The model inputs for the second data-driven model, as shown in Fig. 5, consists of the inputs to the respective FP model ($u_j(t)$), in addition to various other input measurements not used in standalone FP models such as the attemperator spray flowrate, valve openings, and certain inlet steam temperature measurements at specific locations (T_{meas}) for the integrated parallel model (Plant B). The list of the input/output variables considered for the integrated parallel hybrid FP + AI model can be found in Table C1 in Appendix C. The variables involved in the integrated parallel hybrid models represent the same input/output operational variables in the parallel framework, as compared to the individual integrated hybrid FP + AI models and, therefore, not re-defined in Table C1.

The temporal variations of steam inlet temperatures, over a continuous period of 27 days of plant operation, at a couple of locations (referred to as 'Inlet 1' and 'Inlet 2') on the inlet side of the superheater system at Plant B have been shown in Fig. C2 in Appendix C. The training data for the AI models in this case are prepared by considering packets of 12-hr operational data. For example, the available data for the entire duration of plant operation under consideration (say, 27 days) are distributed into smaller packets, each spanning a continuous duration of approximately 12 h based on the steady-state plant load characteristics. Thereafter, around 60 % of the total number of those 12-hr packets have been considered for training the data-driven models, followed by a k-fold cross validation step to remove any potential bias in data selection. The predictive performances of the hybrid integrated-parallel FP + AI models have been analyzed while modeling the temporal steam outlet temperatures at individual tube assemblies over a continuous duration of around 27 days, similar to the integrated hybrid models. The steam outlet temperature profiles also portray a considerably higher degree of fluctuations during transients due to variation of plant load frequently cycling among low (450 MW), medium (500 MW) and high (760 MW) load values, as shown in Fig. B2 in Appendix B.

Fig. 15 shows the comparison between the integrated parallel hybrid FP + NN and FP + BML models in predicting the steam outlet temperatures distribution along the width direction of the superheater system in Plant B. As before, only two of those locations (tube assemblies) are chosen for demonstration which correspond to the highest and lowest numerical temperature measurements among all tube assemblies. From Fig. 15, it can be observed that the hybrid FP + NN model relatively outperforms the hybrid FP + BML model in terms of overall RMSE values and associated computational expense during model training, as shown in Table 4. Similar, to the prediction of main steam outlet temperature for the superheater system at Plant A, for this case as well, it is observed that the all-nonlinear parallel (NLS || NLD) static-dynamic NN model (as shown in Fig. 1 (c)) performed superior compared to the NLS-NLD or NLD-NLS models and hence, has been chosen to represent the NN model in the hybrid integrated parallel FP + NN structure.

From Table 4, the RMSE values obtained from the hybrid FP + NN model for predicting the steam outlet temperatures at both locations fall within the permissible limits considered in this work. However, the corresponding results obtained from the hybrid FP + BML model slightly exceed the acceptable RMSE value of 5 °C. It should also be noted that the MAIE values observed for this specific case study example are significantly higher than the desired permissible limit defined for this study. Nevertheless, the integrated parallel hybrid FP + AI models

본 연구는 고온 증기 시스템(슈퍼히터)의 동적 거동을 정확히 예측하기 위한 **하이브리드 First-Principles(FP) + AI 모델**을 개발하고, 그 성능을 NGCC 및 PC 보일러 시스템 두 곳에서 실증하였다.
주요 기여는 다음과 같다:

1. **세 가지 하이브리드 구조(직렬, 병렬, 통합형)**를 비교 분석하였으며, 각 구조는 시스템 특성과 데이터 품질에 따라 장단점을 지님.
2. **AI 모델로는** 정적-동적 시계열 신경망(NN)과 BML(Bayesian Machine Learning)을 활용하여 **정확도와 불확실성 처리 성능을 비교**함.
3. 실제 플랜트 데이터를 기반으로, 하이브리드 모델은 기존 FP 단독 모델보다 **예측 정확도(RMSE 기준)가 10배 이상 향상**됨.
   - 예: FP 모델의 RMSE가 12.3° C → FP+AI 모델은 0.5° C
4. 하이브리드 모델은 **시간적/공간적 분포 예측에도 효과적**이어서, 향후 **실시간 감시 시스템이나 디지털 트윈 기반 운영 최적화**에도 응용 가능성이 있음.

이러한 결과는 **하이브리드 모델이 고온 열교환기 구성 요소의 정확한 상태 예측 및 모니터링을 위한 강력한 도구가 될 수 있음**을 보여준다.

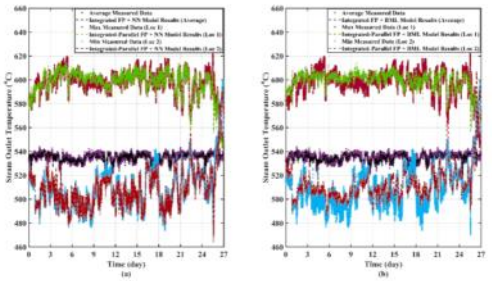

Fig. 15. Comparison of results between hybrid integrated-parallel (a) FF + NN and (b) FF + RML models for predicting steam outlet temperatures along width direction with respect to Plant B.

Table 4
Comparison between FF + NN and FF + RML models in terms of RMSE, MAIE, and computational expense for predicting steam outlet temperatures in Plant B at individual flow circuits along the width direction.

Types of Models	Location 1 (Loc 1)		Location 2 (Loc 2)		Training Computational Time for respective AI models
	RMSE (°C)	MAIE (°C)	RMSE (°C)	MAIE (°C)	
FF + NN	3.1	23.3	3.6	21.5	2 min
FF + RML	6.1	25.7	5.4	27.3	94 min

successfully enhance (as evident from the RMSE values with respect to measured data, refer Table 4) the overall fidelity of the hybrid model by incorporating an additional dimension (variability along width) as compared to the FF model. The higher instantaneous mismatch in the temporal temperature profiles may be attributed to the potential presence of uncertainties in the data under consideration with respect to the coal-fired power plant system (Plant B), stemming from both process noise as well as measurement noise. Furthermore, several other process variables, such as variabilities in coal composition, moisture content, and burner conditions, measurement of which are not available from the industrial partner plant, can significantly impact the temporal temperature profiles.

6.2. Modeling of tube wall and flue gas temperatures

In addition to the steam outlet temperature profiles, the developed hybrid FF + AI models also provides capabilities for representing other process variables such as outer tube metal wall temperatures of superheater tubes and temperature profiles of the flue gas stream.

6.2.1. Results for the average tube wall and flue gas temperatures

Accurate prediction of the transient tube wall temperatures in thermal systems can help to prevent overheating and local hotspots, thus reducing potential failure of superheater tubes. On the other hand, precisely estimating the temporal flue gas temperature profiles can ensure efficient heat recovery in boiler systems and assess internal/external fouling of the tubes, and damage to the refractory. For brevity, the results are presented for only a subset of locations (tags), namely RB 1 for results related to tube wall temperature and G 71′ for those related to flue gas outlet temperatures (please see Fig. 6 (a)).

- *Results from the Series Hybrid FF + AI Models (Plant A)*

Similar to the results obtained from the standalone FF model for the main steam outlet temperature (see Fig. 11), the predictive performance of the FF model for the average tube wall and flue gas temperatures at locations RB 1 and G 71′ (refer Fig. 6 (a)), respectively are shown in Fig. A2 in Appendix A. As mentioned in Section 4.1, Plant A contains 74 flow circuits along the width direction (refer Fig. 6 (b)), out of which 18 flow circuits have temperature data available for tube wall and flue gas temperatures at various locations (refer Fig. 6 (a)). In both Fig. A2 (a) and A2 (b), large discrepancies are observed between the average measured data and the predictions obtained from the FF model. In Fig. A2 (a), the FF model underpredicts the average measured data for the tube temperature at RB 1 with an RMSE of around 12.5 °C, whereas, in Fig. A2 (b), the FF model overpredicts the observed average flue gas temperature at G 71′ with an approximate RMSE of 2.1 °C, spanning for the overall duration of the 20 h used for model simulation. The significantly large plant-model mismatch observed for both these variables can be attributed to various uncertainties associated with the standalone FF model, due to one or more modeling assumption(s) such as ignoring ash fouling of outer tube wall surface and oxide scale deposition inside the tubes. However, as discussed before, it is difficult to develop accurate mechanistic models of some these phenomena such as ash fouling due to uncertainty and complexity of the mechanisms of ash deposit on and removal from the tube outer surfaces. The series hybrid FF + AI

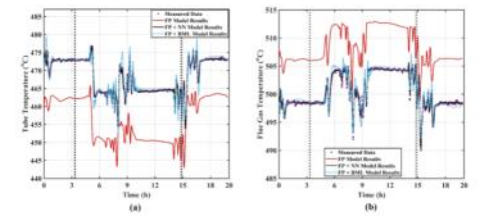

Fig. 16. Comparison of results among standalone FF, FF + NN and FF + RML models with the measured data for Plant A, (a) average tube wall temperature at RB 1 and (b) average flue gas temperature at G 71′ (see Fig. 6).

model described in Section 5.1 has been implemented to address such plant-model mismatches. Also similar to Fig. 11, in the legend "Measured Data" represents the arithmetic average of the actual measured industrial operating data obtained from the plant historian and the legend "FF Model Results" represents the results obtained by simulating the standalone dynamic distributed FF model (refer Section 4.3) for Plant A in absence of any data-driven augmentation.

Similar, to the prediction of the main steam outlet temperature using the series hybrid FF + AI as discussed in Section 6.1.1, the optimal series hybrid FF + AI models also significantly improved the predictive performance of a standalone FF model while estimating the average tube wall temperatures and flue gas temperatures at different locations (see Fig. 6.) of the superheater system at Plant A. Fig. 16 shows the comparison among standalone FF vs FF + NN vs FF + RML models for the average tube wall temperature at RB 1 and the average flue gas temperature at G 71′ of the superheater system at Plant A. As shown previously in Fig. A2, the standalone FF model shows a consistent negative bias with respect to the average temperature measurements at RB 1, and a consistent positive bias with respect to the average temperature measurements at G 71′, thus leading to approximate overall RMSE of 12.3 °C and 8.1 °C, respectively, for both locations during the entire time-series data spanning around 20 h. The accurate prediction of metal temperature of the superheater tubes can be critical for developing a boiler health monitoring framework for assessing and predicting potential tube failures. Therefore, underpredicting or overpredicting the tube and flue gas temperatures may lead to inaccurate failure predictions for superheater tubes and other boiler components. From Fig. 16 (a), it can be seen that results from both hybrid FF + AI models are closer to the real-time plant measurements of the average tube wall temperature at RB 1, thus yielding RMSE values of 0.5 °C and 1.4 °C, for the FF + NN model and the FF + RML model, respectively. Similarly, significant improvement in performance of both hybrid FF + AI models for the average flue gas temperature at G 71′is observed in Fig. 16 (b), with an overall RMSE of 0.4 °C and 0.9 °C for the FF + NN model and the FF + RML model, respectively.

Furthermore, not only does the hybrid FF + NN model yields superior RMSE values as compared to the FF + RML model while modeling the transient average tube wall and flue gas temperature profiles, but it also significantly outperforms the latter in terms of accurately capturing the overshoots and undershoots in the temporal temperature profiles, thus leading to much lesser values of MAIE, as shown in the plots in Fig. A3 and Fig. A4 in Appendix A, illustrating a zoomed portion of training data considered between the 5th and 10th hours of plant operation. While the FF + NN yields the worst-case instantaneous error, i.e., MAIE values of 4.0 °C and 2.8 °C for tube wall and flue gas temperatures respectively for the entire 20 h duration, the FF + RML model yields MAIE values as high as 6.0 °C and 4.8 °C, respectively, for those two output variables, as seen in Table 5. The comparison between the candidate models in terms of various performance measures while predicting the average tube temperature (RB 1) and average flue gas temperature (G 71′) has also been shown in Table 5. Comparison among the candidate hybrid models along with the standalone FF model for predicting the average tube wall temperatures and average flue gas temperatures at other locations (see Fig. 6 (a)) in the Plant A superheater has been included in Fig. A3 through Fig. A6 in Appendix A. Comparison for the validation data at the other locations have been shown in Table A3 in Appendix A. From Table A3, it is evident that both types of hybrid FF + AI models significantly improve the predictive capabilities as compared to the standalone FF model. Furthermore, for this case study, the FF + NN model yields superior RMSE and MAIE values for both the training

Table 5
Comparison among FF, FF + NN, and FF + RML models in terms of RMSE, MAIE, number of parameters and training computational time for average tube temperature (RB 1) and average flue gas outlet temperature (G 71′) in Plant A.

Types of Model	Number of Model Parameters	Training Computational Time for respective AI models	Average Tube Wall Temperature at RB 1 (°C)		Average Flue Gas Outlet Temperature at G 71′(°C)	
			RMSE	MAIE	RMSE	MAIE
FF	-	-	12.3	25.6	8.1	16.0
FF + NN	182	2.3 min	0.5	4.0	0.4	2.8
FF + RML	186	21.7 h	1.4	6.0	0.9	4.8

and validation data compared to the FP + BML model.

The complete list of all optimal candidate basis functions estimated for this case study by the BML algorithms, as well as their applicability to model variables, is shown in Tables A1 and A2 in Appendix A. The computational time associated with the training of the NN model (2.3 min) for implementation in the hybrid FP + AI framework is also significantly lesser than that of the BML model (21.7 h), due to the branch and bound algorithm involved in the BIDGAM approach for selection of optimal set of basis functions. However, it is to be noted that the hybrid FP + BML model exhibits superior model sparsity and hence, considers significantly lesser number of parameters than the FP + NN model while modeling the final superheater system at Plant A. This, in turn, leads to a slightly higher value of the corrected Akaike information criteria (6,7,8) (AICc) obtained for the optimal FP + NN model ($AIC_c = 3047$) when compared to that calculated for the optimal FP + BML model ($AIC_c = 2978$) with respect to the system under consideration. Minimizing the AICc during parameter estimation in data-driven models penalizes overfitting during model training, thus leading to a parsimonious model structure.

6.2.2. Results for the Spatio-Temporal distribution of tube wall temperature

The superheater system in Plant A consists of 74 flow circuits (see Fig. 6 (b)) along the width direction. Hence, like Plant B as discussed in Section 6.1.3, constructing an accurate first-principles model for each flow circuit along the width direction (refer Fig. 6 (b)) for this system can also be computationally expensive.

★ Results from the Series Parallel Hybrid FP + AI Models (Plant A)

Table C3 in Appendix C shows the temperature distribution in the width direction for tube wall temperature at location E 75′ (refer Fig. 6 (a)) for Plant A. As seen in Fig. C3, the measured temperature data for different flow circuits at location E 75′ shows a significant variance in tube temperature measurements.

For Plant A, the series hybrid model considered to predict the average measured temperatures at all locations for which measured data are available in Plant A has also been coupled with a second AI model in parallel thus leading to the series parallel hybrid FP + AI structure. Similar to the integrated parallel model used for Plant B (refer Section 6.1.2) the series parallel model developed are then implemented for modeling the dynamic temperature profiles along the width direction of the superheater systems in Plant A. Similar to the integrated parallel hybrid FP + AI model developed for Plant B, the target dynamic outputs of the second AI models for series parallel hybrid model as shown in Fig. 5, is given by Eq. (12). Table C2 in Appendix C lists the input/output variables. Again, like the integrated parallel hybrid model the variables involved in the series hybrid model represent exactly the same input/output operational variables in the parallel framework, as compared to the individual series FP + AI models and, therefore, not re-defined in Table C2.

The results obtained from the series parallel hybrid FP + AI models considers the same duration of training data as compared to the series hybrid FP + AI models. However, in addition to the four inputs (i.e. $T_{exh}, \dot{m}_{st}, T_{fg,in}, \dot{m}_{fg}$) considered previously for the series hybrid model, the reheater mass flowrate ($\dot{m}_{fg}$) is considered as an additional input variable for the development of the second AI models ($u_{AI,2}(t)$). The temporal profile of $\dot{m}_{fg}$ during the entire 20 h operating period for Plant A has been shown in Fig. C4 in Appendix C. It is noted that measurements are available for Plant A from thermocouples installed on 10 different

Table 6
Comparison between FP + NN and FP + BML models in terms of RMSE and MAIE for prediction of the distribution of tube wall temperature (E 75′) in Plant A.

Types of Models	Location 1 (Loc 1)		Location 2 (Loc 2)	
	RMSE (°C)	MAIE (°C)	RMSE (°C)	MAIE (°C)
FP + NN	0.4	3.0	0.3	2.6
FP + BML	1.0	3.7	1.0	6.7

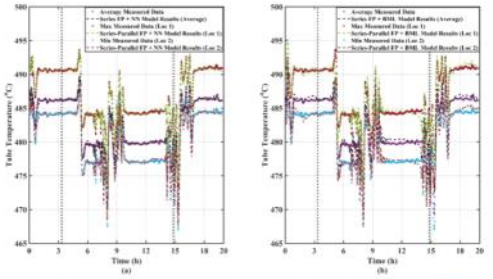

Fig. 17. Comparison of results between hybrid series–parallel (a) FP + NN and (b) FP + BML models for tube temperatures at E 75′ location (refer Fig. 6) in Plant A.

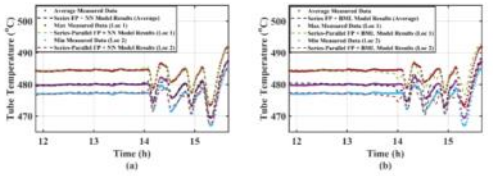

Fig. 18. Comparison of results between hybrid series–parallel (zoomed section) (a) FP + NN and (b) FP + BML models for tube temperatures at E 75′ (refer Fig. 6 (a)) for Plant A.

flow circuits along each location/elevation (see Fig. 6 (b)), out of which two tube assemblies are chosen for analyses which recorded the highest and lowest temperature values at the respective elevations across all 18 circuits. Fig. 17 shows the comparison between the hybrid series parallel FP + NN (Fig. 17 (a)) vs FP + BML (Fig. 17 (b)) models for prediction of the tube temperature distribution along the width direction at E 75′. The black dotted vertical lines in Fig. 17 indicate the duration of training data. The comparison of RMSE and MAIE for the temporal temperature distribution of tube wall at E 75′ between both types of series parallel hybrid models for both 'Loc 1' and 'Loc 2' is shown in Table 6.

As can be seen in Table 6, both types of hybrid FP + AI models improve the overall predictive performance yielding acceptable values of RMSE and MAIE. Although both types of series parallel hybrid models satisfactorily match the trends in the temporal temperature profiles at both locations (referred to as 'Loc 1' and 'Loc 2') as shown in Fig. 17, the FP + NN model slightly outperforms the FP + BML model, especially in terms of accurately capturing the overshoots and undershoots during transients as seen in the zoomed section plots in Fig. 18 for the E 75′ location. Furthermore, the FP + NN model also yields slightly superior RMSE and MAIE as compared to the FP + BML model not only while predicting the tube temperatures at E 75′, but also at the other elevations for which tube temperature and flue gas temperature measurements are available, as can be seen in Table C3 in Appendix C. The plots comparing model performance for the validation data of other locations are shown in Fig. C5 through Fig. C10 in Appendix C.

Comparisons between the NN and BML models used in the series parallel hybrid FP + AI framework in terms of the number of parameters (model sparsity) and overall training computational time has been included in Table C4 in Appendix C. Furthermore, the optimal set of candidate basis functions selected by both BML models as well as their applicability to model variables with respect to Plant A has been listed in Tables C5 and C6 in Appendix C.

7. Conclusions

All three types of hybrid models developed in this paper, i.e., series, integrated, and parallel structures, significantly outperform the standalone FP model while modeling the final superheater systems of the combined cycle (Plant A) and coal-fired (Plant B) power plants. For instance, while the standalone FP model developed for the superheater system at Plant A yielded RMSE and MAIE values as high as 12.3 °C and 25.6 °C, respectively, while predicting the transient average tube wall temperature at RB 1, the series hybrid FP + AI model yields RMSE values of 0.5 °C (FP + NN) and 1.4 °C (FP + BML), and MAIE values of 4.0 °C (FP + NN) and 6.0 °C (FP + BML), respectively. For this case study, the series hybrid FP + NN model prominently outperforms the FP + BML model in terms of predictive accuracy and computational expense while predicting the dynamic temperature profiles of all output variables considered, but the NN model has considerably greater (162 vs 196) number of model parameters. On the contrary, both hybrid FP + AI models show similar predictive performance in terms of RMSE (around 1.9–2.0 °C) and MAIE (around 6.5–8.5 °C) values for the main steam outlet temperature of Plant B through the integrated framework, but the optimal BML model has less than one-third of the number of parameters compared to the optimal NN model. It is worth mentioning that the computational time involved for the training of the NN models in all hybrid FP + AI structures discussed in this paper is considerably lower than that of the BML models mainly due to the time taken for solving the mixed integer nonlinear programming problem for selection of optimal set of candidate basis functions and parameter estimation in the BML algorithm. The computational expense associated with the BML models can eventually be reduced by leveraging parallel computing approaches in the BIDGAM algorithm. On the other hand, the sequential training algorithms for the all-nonlinear static-dynamic NN models ensure faster convergence within the hybrid framework, even for highly nonlinear transient data.

The parallel (series-parallel and integrated-parallel) hybrid FP + AI models are found to accurately capture the spatio-temporal variations in the tube wall/flue gas and steam outlet temperature profiles along the width direction of the superheater systems at Plants A and B. For all these case studies, the optimal hybrid FP + BML models consistently show superior model sparsity and interpretability, whereas the hybrid FP + NN models exhibit consistent superior performance, if not similar, in terms of predictive capabilities and computational expense during model development.

Finally, the authors would like to note that it is considerably difficult to arrive at a universal conclusion on the superiority of a particular type of hybrid FP + AI model over another since the efficiency of such synergistic integration of FP and AI models largely depend on several factors such as the physics/chemistry of the specific system, type of

information transferred between the models, characteristics of data available for training the data-driven models, and candidate architectures/algorithms associated with the development of the hybrid framework. In general, it is our opinion that for modeling complex dynamic systems, various structures of the hybrid FP + AI models can be exploited without necessarily developing a very high-fidelity FP model that may require large resources and can incur excessive computational cost. Although, the fidelity of the FP model and the capability/characteristics of the AI models depend on specific system and the variables to be represented by the hybrid models. We believe that the proposed hybrid FP + AI structures and AI models exhibit sufficient flexibilities to be implemented independently or in combination with one another, not only for modeling industrial superheater systems, but also many other complex dynamic nonlinear systems.

Declaration of competing interest

The authors declare that they have no known competing financial interests or personal relationships that could have appeared to influence the work reported in this paper.

Acknowledgements

The project is funded by the U.S. DOE through the project titled "Boiler Health Monitoring Using a Hybrid First Principles – Artificial Intelligence Model" (Grant # DE – FE0031766). The DOE financial support is gratefully acknowledged.

Appendix A

Additional plots and tables showing temporal distributions of input variables and results from the series hybrid FP + AI Models with respect to Plant A.

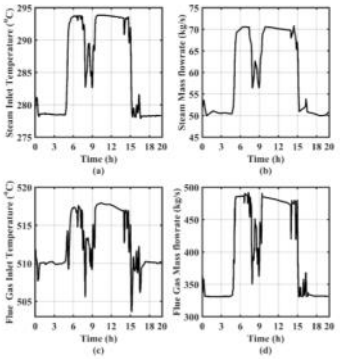

Fig. A1. Dynamic profiles of input variables for Plant A final superheater system considered for the standalone FP model, i.e., (a) steam inlet temperature ($T_{w,in}$), (b) steam mass flowrate ($\dot{m}_w$), (c) flue gas inlet temperature ($T_{fg,in}$), and (d) flue gas mass flowrate ($\dot{m}_{fg}$) (see Fig. 9 (a)).

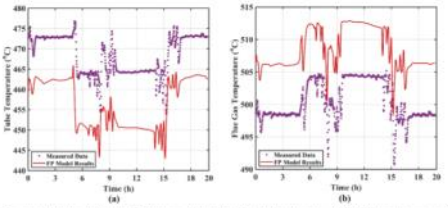

Fig. A2. Comparison of results from the standalone FP model vs measured data in Plant A for, (a) tube wall temperature at RS 1 and (b) flue gas temperature at G.T1, (refer Fig. 6)

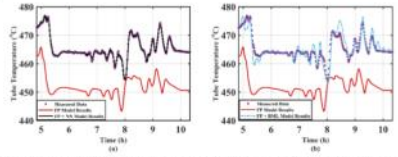

Fig. A3. Comparison of results among standalone FP and hybrid (a) FP+SN and (b) FP+BML models with measured data for tube wall temperature at RS 1 (see Fig. 6) for Plant A.

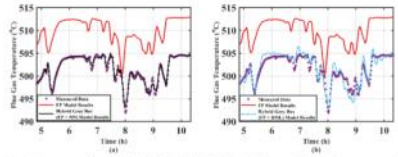

Fig. A4. Comparison of results among standalone FP and hybrid (a) FP+SN and (b) FP+BML models with measured data for flue gas temperature at G.T1 (see Fig. 6 (a)) for Plant A.

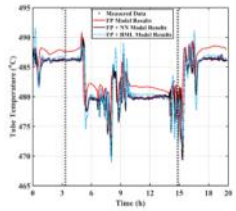

Fig. A5. Comparison of results among standalone FP, FP + NN and FP + RML models with the measured data for tube wall temperature at E 75° (see Fig. 6 (a)) for Plant A.

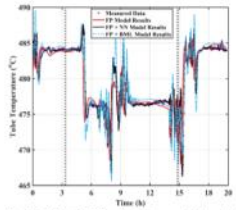

Fig. A6. Comparison of results among standalone FP, FP + NN and FP + RML models with the measured data for tube wall temperature at E 60° (see Fig. 6 (a)) for Plant A.

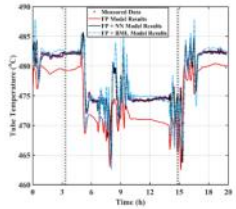

Fig. A7. Comparison of results among standalone FP, FP + NN and FP + RML models with the measured data for tube wall temperature at E 6° (see Fig. 6 (a)) for Plant A.

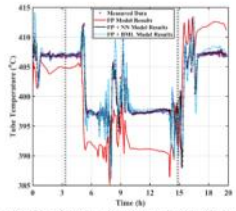

Fig. A8. Comparison of results among standalone FP, FP + NN and FP + RML models with the measured data for tube wall temperature at RH 2 (see Fig. 6 (a)) for Plant A.

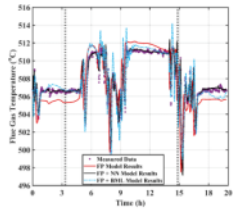

Fig. A9. Comparison of results among standalone FP, FP+NN and FP+RNL models with the measured data for flue gas temperature at G 47' (see Fig. 6 (a)) for Plant A.

Table A1
List of optimal combinations of selected basic functions for the RNL model in series hybrid FP + AI structure while modeling the superheater system at Plant A.

Types of Nonlinear Combinations	List of Optimal Basis Functions selected during Training
Bilinear	$x_2x_3, x_2x_4, x_3x_4, x_3x_5, x_4x_5, x_5x_6, x_5x_{10}$
Inverse/Reciprocal	$\frac{1}{x_{10}}$
Sigmoid	$\frac{1}{1+\exp(-x_6)}$

Table A2
Physical significances of all input/output variables used in the basic functions of RNL model in series hybrid FP + AI structure while modeling the superheater system at Plant A.

Input/Output Variables	Physical significance with respect to Superheater System at Plant A
x_1	m_{ss}(inlet mass flowrate of steam)
x_2	m_{fg}(inlet mass flowrate of flue gas)
x_3	T_{ss}(inlet temperature of steam)
x_4	T_{fg}(inlet temperature of flue gas)
x_5	$T_{Steam,FP}$(main steam outlet temperature predicted by FP model)
x_6	$T^{FP}_{Wall,6'6''}$(average tube temperature at S 7'6" predicted by FP model)
x_7	$T^{FP}_{Wall,E49'}$(average tube temperature at E 49' predicted by FP model)
x_8	$T^{FP}_{Wall,6'}$(average tube temperature at S 6' predicted by FP model)
x_9	$T^{FP}_{Wall,RB2}$(average tube temperature at RB 1 predicted by FP model)
x_{10}	$T^{FP}_{Wall,RB2}$(average tube temperature at RB 2 predicted by FP model)
x_{11}	$T^{FP}_{Gas,G71'}$(average flue gas outlet temperature at G 71' predicted by FP model)
x_{12}	$T^{FP}_{Gas,G47'}$(average flue gas outlet temperature at G 47' predicted by FP model)
y_1	$\delta_{Steam,RNL}$(residual in main steam outlet temperature predicted by RNL model)
y_2	$\Delta^{RNL}_{Wall,6'6''}$(residual in avg tube temperature at S 7'6" predicted by RNL model)
y_3	$\Delta^{RNL}_{Wall,E49'}$(residual in avg tube temperature at E 49' predicted by RNL model)
y_4	$\Delta^{RNL}_{Wall,6'}$(residual in avg tube temperature at S 6' predicted by RNL model)
y_5	$\Delta^{RNL}_{Wall,RB1}$(residual in avg tube temperature at RB 1 predicted by RNL model)
y_6	$\Delta^{RNL}_{Wall,RB2}$(residual in avg tube temperature at RB 2 predicted by RNL model)
y_7	$\Delta^{RNL}_{Gas,G71'}$(residual in avg flue gas outlet temperature at G 71' predicted by RNL model)
y_8	$\Delta^{RNL}_{Gas,G47'}$(residual in avg flue gas outlet temperature at G 47' predicted by RNL model)

Table A3
Comparison among FP, FP + NN, and FP + RNL models in terms of RMSE and MAPE for average tube wall temperatures and average flue gas temperatures (see Fig. 6 (a)) for Plant A.

Average Temperature Location	Types of Models	RMSE (°C)	MAPE (%)
S 7'6"	FP	2.9	12.0
	FP + NN	2.4	1.7
	FP + RNL	1.1	0.4
E 49'	FP	2.3	11.5
	FP + NN	0.3	4.4
	FP + RNL	1.3	0.1
S 6'	FP	3.8	14.7
	FP + NN	0.5	3.6
	FP + RNL	1.4	0.2
RB 2	FP	0.6	10.8
	FP + NN	0.6	2.2
	FP + RNL	1.3	0.8
G 47'	FP	2.5	10
	FP + NN	0.4	3.2
	FP + RNL	1.3	4.2

Appendix B

Additional plots and tables showing temporal distributions of input variables and results from integrated hybrid FP + AI Models with respect to Plant B.

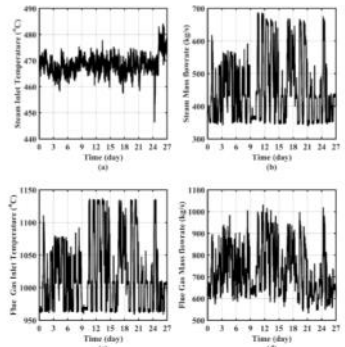

Fig. B1. Dynamic profiles of input variables for Plant B final superheater system considered for standalone FP model, i.e., (a) steam inlet temperature ($T_{ss,fp}$), (b) steam mass flowrate ($\dot{m}_{ss}$), (c) flue gas inlet temperature ($T_{fg,fp}$), and (d) flue gas mass flowrate ($\dot{m}_{fg}$) (see Fig. 8 (b))

The quadratic correlation for relating inlet flue gas temperature with plant load is:

$$y = 0.005^*x^2 + 0.2762^*x + 1543.5 \quad \text{(B1)}$$

where, x = Plant Load (MW), y = Inlet Flue Gas Temperature (°F).

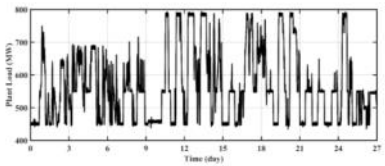

Fig. B2. Temporal profiles of the plant load among low, medium, and high values for the superheater system at Plant B.

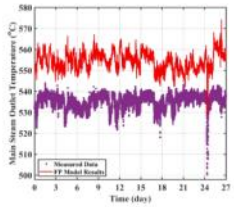

Fig. B3. Comparison of results from the standalone FP model with the measured data for main steam outlet temperature with respect to Plant B.

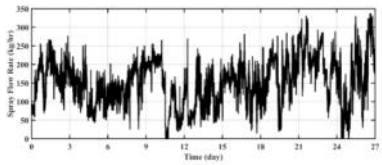

Fig. B4. Temporal profiles of attemperator spray flow rate ($\dot{m}_{spray}$) considered as additional input for the AI models with respect to Plant B for the integrated hybrid FP-i AI structure.

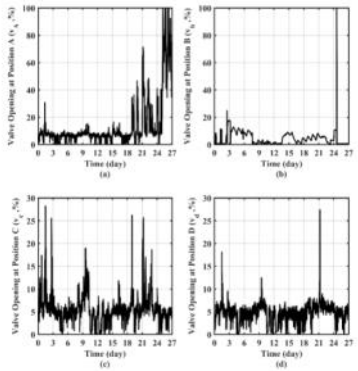

Fig. B5. Temporal profiles of input variables, i.e., valve openings at (a) Position A (v_{PA}), (b) Position B (v_{PB}), (c) Position C (v_{PC}), and (d) Position D (v_{PD}), considered as additional inputs for the AI models for Plant B for the integrated hybrid FP-i AI structure.

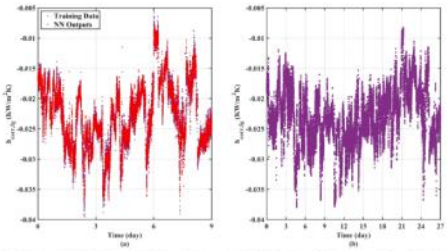

Fig. B6. (a) Training results for NN model for randomly chosen 9 days from the entire 27-day duration, and (b) prediction results from the NN model, while estimating $h_{conv,fg}$ with respect to the integrated hybrid FP+NN structure for implementation in Plant B.

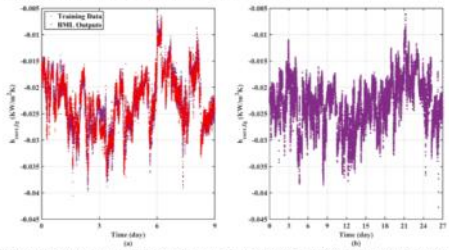

Fig. B7. (a) Training results for RML model for randomly chosen 9 days from the entire 27-day duration, and (b) prediction results from the RML model, while estimating $h_{conv,fg}$ with respect to the integrated hybrid FP+RML structure for implementation in Plant B.

Table B1
List of model input and output variables in the integrated hybrid FP + AI models for the superheater system of Plant B.

Variables used in Fig. 3.	Actual input/output variables for the integrated hybrid FP + AI model in terms of process variables for Plant B
$u_1(t)$	$T_{exh}, \dot{m}_{fw}, T_{fgin}, \dot{m}_{fg}$
$Y_{out}(t)$	$h_{conv,fg}$(for data preparation during training) No $Y_{out}(t)$ during simulation
$u_{out}(t)$	$\dot{m}_{spray}, \gamma_{1,1}, \gamma_{1,2}, \gamma_{2,1}, \gamma_{2,2}$

(continued on next page)

Table B1 (continued)

Variables used in Fig. 3.	Actual input/output variables for the integrated hybrid FP + AI model in terms of process variables for Plant B
$Y_{out}(t)$	$h_{conv,fg}$(during simulation)
$Y_{out,lag}(t)$	T_{exhin}

Table B2
Mathematical representations of optimal NN and RML models obtained for the integrated hybrid FP + AI structure while modelling the superheater system at Plant B.

Optimal AI models	Mathematical representations
NN	$h_{conv,fg} = \phi_2(W_{out}\phi_1(W_{hid}[u_1(t) \; u_2(t) \; Y_{out}(t)]^T + \beta_1) + \beta_2)(t) = \frac{1}{1+\exp(-x)}$, $x_{out} = \begin{bmatrix} W_{hid} = \begin{bmatrix} 12.80 & -1.67 & -3.56 & -13.09 & -7.71 & -1.63 & -1.90 & 5.81 & 1.62 \\ 153.54 & -42.28 & 6.67 & -124.04 & 6.04 & -10.77 & 7.81 & 5.13 & -0.38 \\ 91.16 & 8.17 & -11.21 & -89.15 & 0.62 & 9.84 & 0.27 & 2.87 & 0.89 \\ 33.70 & 49.86 & 1.11 & 0.36 & 2.73 & 0.13 & 6.08 & -7.25 & 10.38 \\ 69.76 & -2.19 & 4.12 & 87.18 & 2.99 & 9.31 & 1.32 & 3.43 & 0.47 \\ 22.87 & -3.26 & 3.67 & 7.13 & -4.92 & -13.31 & 3.70 & 4.27 & 3.26 \\ 82.23 & 2.40 & -11.71 & 29.84 & 8.31 & 23.00 & 4.24 & -7.84 & 0.43 \\ -13.86 & 2.85 & -1.24 & 26.91 & 0.60 & 2.62 & 2.19 & -4.68 & 2.83 \\ -3.27 & 3.81 & 3.81 & -2.99 & -1.16 & -1.44 & 2.44 & 0.86 & 0.21 \end{bmatrix}, \\ W_{out} = [2.21 \quad -0.84 \quad 1.29 \quad 0.47 \quad 1.86 \quad 1.31 \quad 0.90 \quad -1.93 \quad 0.97], \\ \beta_1 = [2.04 \quad 0.47 \quad 10.10 \quad -8.14 \quad 2.07 \quad 13.06 \quad 0.64 \quad -7.28 \quad -0.47]^T, \\ \beta_2 = -0.38 \end{bmatrix}$
RML	$h_{conv,fg} = C^T\Psi(u_1, u_2, u_3)$, $\Psi(u_1, u_2, u_3) = [\frac{1}{\sqrt{\sigma_{11}}} \exp(-\frac{1}{2}(\frac{u_1-\mu_{11}}{\sigma_{11}})^2) \; \frac{1}{\sqrt{\sigma_{12}}} \exp(-\frac{1}{2}(\frac{u_2-\mu_{12}}{\sigma_{12}})^2) \; \frac{1}{\sqrt{\sigma_{13}}} \exp(-\frac{1}{2}(\frac{u_3-\mu_{13}}{\sigma_{13}})^2) \; \frac{1}{\sqrt{\sigma_{21}}} \exp(-\frac{1}{2}(\frac{u_1-\mu_{21}}{\sigma_{21}})^2) \; \frac{1}{\sqrt{\sigma_{22}}} \exp(-\frac{1}{2}(\frac{u_2-\mu_{22}}{\sigma_{22}})^2) \; \frac{1}{\sqrt{\sigma_{23}}} \exp(-\frac{1}{2}(\frac{u_3-\mu_{23}}{\sigma_{23}})^2)]$ $C = [7.57 \quad 40.24 \quad -13.42 \quad 2.09 \quad 28.14 \quad 19.99 \quad 11.49 \quad -3.17 \quad 1.36 \quad -17.33 \quad -63.81 \quad 24.38 \quad 6.32 \quad 0.48 \quad -1.48 \quad 43.06 \quad 21.22 \quad 27.06 \quad 10.93 \quad 32.80 \quad -5.02 \quad -1.43 \quad -49.31 \quad 56.84 \quad 12.74 \quad -3.94 \quad 0.67]$ Note that the dimension of $\Psi_{1\times m}$ is 27x1 (column vector) and that of C is 1x27 (row vector).

Note: All input and output variables in Table B2 are normalized.

Appendix C

Additional plots and tables showing temporal distributions of input variables and results from parallel hybrid FP + AI Models with respect to Plant A and Plant B.

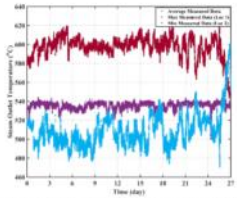

Fig. C1. Distribution of transient steam outlet temperature profiles for Plant B, across the flow circuits/locations along the width direction

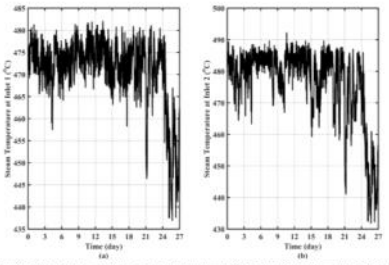

Fig. C2. Dynamic profiles of the additional input variables, i.e., steam inlet temperatures at (a) 'Inlet 1' and (b) 'Inlet 2' considered in the AI models for the integrated parallel hybrid PP+AI structure for Plant B.

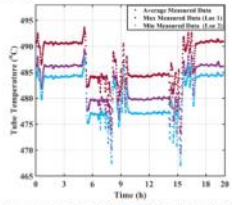

Fig. C3. Distribution of transient tube wall temperature profiles at E 75' (refer Fig. 6 (a)) with respect to Plant A across the flow circuits/locations along the width direction

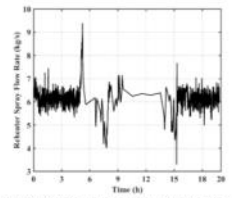

Fig. C4. Dynamic profile of reheater spray mass flow rate ($\dot{m}_{rs}$) considered as an additional input in the AI models of Plant A for the series parallel hybrid PP+AI structures.

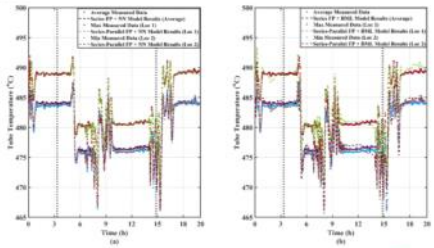

Fig. C5. Comparison of results between series parallel hybrid (a) PP+NN and (b) PP+RML models for tube temperatures at E 49' (see Fig. 6 (a)) for Plant A.

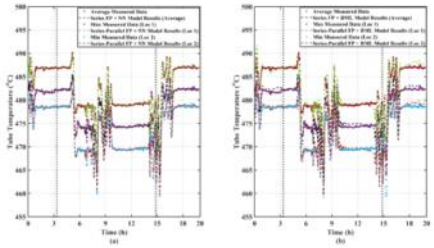

Fig. C6. Comparison of results between series parallel hybrid (a) FP+NN and (b) FP+RML models for tube temperatures at E 6' (see Fig. 6 (a)) for Plant A.

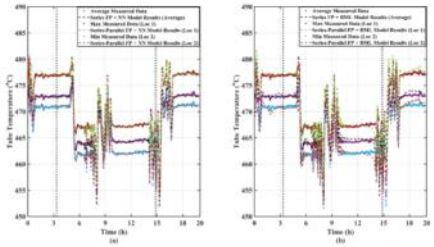

Fig. C7. Comparison of results between series parallel hybrid (a) FP+NN and (b) FP+RML models for tube temperatures at RR 1 (see Fig. 6 (a)) for Plant A.

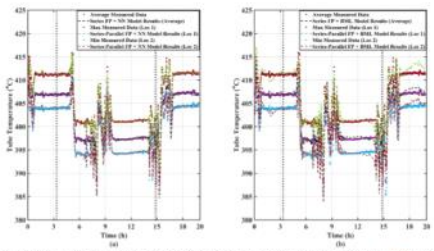

Fig. C8. Comparison of results between series parallel hybrid (a) FP+NN and (b) FP+RML models for tube temperatures at RR 2 (see Fig. 6 (a)) for Plant A.

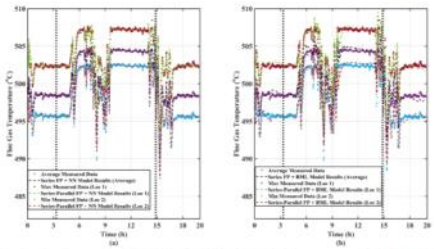

Fig. C9. Comparison of results between series parallel hybrid (a) FP+NN and (b) FP+RML models for flue gas temperatures at G 7'C' (see Fig. 6 (a)) for Plant A.

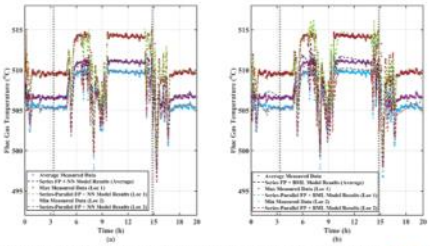

Fig. C10. Comparison of results between series parallel hybrid (a) FP+NN and (b) FP+BML models for flue gas temperatures at G 47° (see Fig. 6 (a)) for Plant A.

Table C1
List of model input and output variables in the integrated-parallel hybrid FP + AI models for the superheater system of Plant B.

Variables used in Fig. 3 (b)	Actual input/output variables for the integrated-parallel hybrid FP + AI model in terms of process variables for Plant B
$u_1(t)$	$\dot{m}_{sh}, T_{sh}, T_{fg1}, \dot{m}_{fg}$
$y_{1,BML_1}(t)$	T_{metal}
$u_{2,BML}(t)$	$\dot{m}_{spray}, T_{fg1}, T_{fg2}, T_{fg3}, T_{fg4}$
$y_{1,BML}(t)$	$\dot{m}_f$
$y_{2,BML_2}(t)$	T_{fg5}

Table C2
List of model input and output variables in the series-parallel hybrid FP + AI models for the superheater system of Plant A.

Variables used in Fig. 5 (a)	Actual input/output variables for the series-parallel hybrid FP + AI model in terms of process variables for Plant A
$u_1(t)$	$T_{sh}, \dot{m}_{sh}, T_{fg1}, \dot{m}_{fg}$
$y_{1,BML_1}(t)$	$T_{metal}, T_{fg2}^{FP}, T_{fg3}^{FP}, \dot{m}_f^{FP}, T_{fg4}^{FP}, T_{fg5}^{FP}, T_{fg6}^{FP}, T_{fg7}^{FP}, T_{fg8}^{FP}$
$u_{2,BML}(t)$	$\dot{m}_{spray}$
$y_{1,BML}(t)$	$T_{fg2}, T_{fg3}^{BML}, T_{fg4}^{BML}, T_{fg5}^{BML}, T_{fg6}^{BML}, T_{fg7}^{BML}, T_{fg8}^{BML}$
$y_{2,BML_2}(t)$	$T_{fg2}, T_{fg3}^{BML}, T_{fg4}^{BML}, T_{fg5}^{BML}, T_{fg6}^{BML}, T_{fg7}^{BML}, T_{fg8}^{BML}$

Table C3
Comparison between FP + NN and FP + BML models in terms of RMSE and MAPE for tube wall and flue gas temperatures at individual locations along width direction with respect to Plant A.

Temperature Location	Types of Models	Location 1 (Loc 1)		Location 2 (Loc 2)	
		RMSE (°C)	MAPE (°C)	RMSE (°C)	MAPE (°C)
E 49°	FP + NN	0.9	4.9	0.7	7.8
	FP + BML	1.8	7.2	1.1	8.5
E 6°	FP + NN	0.8	4.2	0.8	4.2
	FP + BML	1.3	6.3	1.2	6.9
RH 1	FP + NN	0.3	2.7	0.7	8.9
	FP + BML	1.4	7.6	1.3	7.2

(continued on next page)

Table C3 (continued)

Temperature Location	Types of Models	Location 1 (Loc 1)		Location 2 (Loc 2)	
		RMSE (°C)	MAPE (°C)	RMSE (°C)	MAPE (°C)
RH 2	FP + NN	0.3	2.8	0.8	10.3
	FP + BML	1.7	8.5	1.4	8.0
G 71°	FP + NN	0.4	3.0	0.4	2.7
	FP + BML	0.8	4.6	0.8	5.2
G 47°	FP + NN	0.4	3.0	0.6	8.0
	FP + BML	1.0	5.2	0.8	4.1

Table C4
Comparison between NN and BML models for the series parallel hybrid FP + AI structure in terms of training computational time and number of parameters.

Types of AI Model for Series-Parallel FP + AI Structure	Number of Model Parameters	Overall Training Computational Time
NN	298	3 min
BML_1	112	233 min
BML_2	126	189 min

Note that two different BML models (BML_1 and BML_2) are simultaneously and independently trained, thus collectively representing the second AI model block in Fig. 5 (b). While BML_2 provides dynamic predictions for all temperatures at 'Loc 1' for all variables, BML_2 provides corresponding predictions at 'Loc 2' for all variables.

Table C5
List of optimal combinations of selected basis functions for the BML models in series parallel hybrid FP + AI structure while modeling the superheater system at Plant A.

Types of BML Model	Set of Optimal Candidate Basis Functions selected during Training
BML_1	$\sqrt{u_4}, u_1^2, u_1 y_7, \frac{1}{u_1}, u_2 u_4^2, \frac{1}{u_1}, \frac{1}{\sqrt{u_1}}, \frac{1}{u_1^2}, u_1$
BML_2	$u_4 u_3, \sqrt{u_2}, u_2, u_2 u_3, \log(u_1), \frac{1}{u_2}, u_2^2, u_2^2, u_2 u_3, \frac{1}{u_2}$

Table C6
Physical significances of all input/output variables used in the basis functions of BML models in series parallel hybrid FP + AI structure while modeling the superheater system at Plant A.

Input/Output Variables	Physical significance with respect to superheater system at Plant A
u_1	$\dot{m}_{sh}$(inlet mass flow rate of steam)
u_2	$\dot{m}_{fg}$(inlet mass flow rate of flue gas)
u_3	T_{sh1}(inlet temperature of steam)
u_4	T_{fg1}(inlet temperature of flue gas)
u_5	$\dot{m}_{sp}$(inlet mass flow rate of reheater spray)
$y_1(BML_1)$	$A_{BML_1,BML}^{FP} - \frac{\dot{m}_{BML_1,max}^{FP}}{\dot{m}_{BML_1,max}^{BML}} T_{BML_1,BML}^{BML}$
$y_2(BML_1)$	$A_{BML_2,BML}^{FP} - \frac{\dot{m}_{BML_2,max}^{FP}}{\dot{m}_{BML_2,max}^{BML}} T_{BML_2,BML}^{BML}$
$y_3(BML_1)$	$A_{BML_3,BML}^{FP} - \frac{\dot{m}_{BML_3,max}^{FP}}{\dot{m}_{BML_3,max}^{BML}} T_{BML_3,BML}^{BML}$
$y_4(BML_1)$	$A_{BML_4,BML}^{FP} - \frac{\dot{m}_{BML_4,max}^{FP}}{\dot{m}_{BML_4,max}^{BML}} T_{BML_4,BML}^{BML}$
$y_5(BML_1)$	$A_{BML_5,BML}^{FP} - \frac{\dot{m}_{BML_5,max}^{FP}}{\dot{m}_{BML_5,max}^{BML}} T_{BML_5,BML}^{BML}$
$y_6(BML_1)$	$A_{BML_6,BML}^{FP} - \frac{\dot{m}_{BML_6,max}^{FP}}{\dot{m}_{BML_6,max}^{BML}} T_{BML_6,BML}^{BML}$
$y_7(BML_1)$	$A_{BML_7,BML}^{FP} - \frac{\dot{m}_{BML_7,max}^{FP}}{\dot{m}_{BML_7,max}^{BML}} T_{BML_7,BML}^{BML}$
$y_8(BML_1)$	$A_{BML_8,BML}^{FP} - \frac{\dot{m}_{BML_8,max}^{FP}}{\dot{m}_{BML_8,max}^{BML}} T_{BML_8,BML}^{BML}$
$y_1(BML_2)$	$A_{BML_1,BML}^{FP} - \frac{\dot{m}_{BML_1,max}^{FP}}{\dot{m}_{BML_1,max}^{BML}} T_{BML_1,BML}^{BML}$
$y_2(BML_2)$	$A_{BML_2,BML}^{FP} - \frac{\dot{m}_{BML_2,max}^{FP}}{\dot{m}_{BML_2,max}^{BML}} T_{BML_2,BML}^{BML}$
$y_3(BML_2)$	$A_{BML_3,BML}^{FP} - \frac{\dot{m}_{BML_3,max}^{FP}}{\dot{m}_{BML_3,max}^{BML}} T_{BML_3,BML}^{BML}$
$y_4(BML_2)$	$A_{BML_4,BML}^{FP} - \frac{\dot{m}_{BML_4,max}^{FP}}{\dot{m}_{BML_4,max}^{BML}} T_{BML_4,BML}^{BML}$
$y_5(BML_2)$	$A_{BML_5,BML}^{FP} - \frac{\dot{m}_{BML_5,max}^{FP}}{\dot{m}_{BML_5,max}^{BML}} T_{BML_5,BML}^{BML}$
$y_6(BML_2)$	$A_{BML_6,BML}^{FP} - \frac{\dot{m}_{BML_6,max}^{FP}}{\dot{m}_{BML_6,max}^{BML}} T_{BML_6,BML}^{BML}$
$y_7(BML_2)$	$A_{BML_7,BML}^{FP} - \frac{\dot{m}_{BML_7,max}^{FP}}{\dot{m}_{BML_7,max}^{BML}} T_{BML_7,BML}^{BML}$

Data availability

All data that have been used have been plotted, provided in tables or text.

References

[1] S. Kuru, M. De Geeter, A. Galetzka, A. Klaeijbe, M. Liebsch, D. Loukrezis, S. Russenschuck, M. Schmidt, Hybrid modeling: towards the next level of scientific computing in engineering, J. Math. Ind. 12 (2022) 8, https://doi.org/10.1186/s13362-022-00125-0.

[2] V. Venkatasubramanian, The promise of artificial intelligence in chemical engineering: is it here, finally? AIChE J. 65 (2019) 466–478, https://doi.org/10.1002/aic.16489.

[3] M. Gnanda, M. Trojan, D. Taler, CFD analysis of steam superheater operation in steady and transient state, Energy 199 (2020) 117423, https://doi.org/10.1016/j.energy.2020.117423.

[4] B. Bahlawg, B.W. Jacobsen, GREY BOX MODELLING – BRANCHES AND EXPERIENCES, IFAC Proc. Vol. 41 (2008) 11413–11420, https://doi.org/10.3182/20080706-5-KR-1001.01914.

[5] V. Saini, O. Bhattacharyya, D. Pandy, J. Parkar, G. Boohaker, Nonlinear state estimation of a power plant superheater by using the extended Kalman filter for differential algebraic equation systems, Appl. Therm. Eng. 251 (2024) 123471, https://doi.org/10.1016/j.applthermaleng.2024.123471.

[6] A. Mukherjee, D. Bhattacharyya, Hybrid series-parallel all-nonlinear dynamic-static neural networks: development, training, and application to chemical processes, Ind. Eng. Chem. Res. 62 (2023) 5221–5237, https://doi.org/10.1021/acs.iecr.3c03309.

[7] S. Adeyemo, D. Bhattacharyya, Optimal nonlinear dynamic sparse model selection and Bayesian parameter estimation for nonlinear systems, Comput. Chem. Eng. 180 (2024) 108502, https://doi.org/10.1016/j.compchemeng.2023.108502.

[8] A. Mukherjee, S. Adeyemo, D. Bhattacharyya, All-nonlinear static-dynamic neural networks versus Bayesian machine learning for data-driven modeling of chemical processes, Can. J. Chem. Eng. (2024), https://doi.org/10.1002/cjce.25379.

[9] M. Mohamadi-Baghmolaei, F. Zahedinaeh, M. Khajeh, S. Zandekhoud, N.M. C. Saadi, Developing a hybridized thermodynamic and data-driven model for catalytic supercritical water gasification of biomass for hydrogen production, Energy Convers. Manage. 307 (2024) 118302, https://doi.org/10.1016/j.enconman.2024.118302.

[10] W. Chen, Y. Liang, X. Luo, J. Chen, Z. Yang, Y. Chen, Artificial neural network gray-box model for design and optimization of 50 MWe-scale combined supercritical CO2 Brayton cycle-ORC coal-fired power plant, Energy Convers. Manage. 249 (2021) 114821, https://doi.org/10.1016/j.enconman.2021.114821.

[11] D.C. Psichogios, L.H. Ungar, A hybrid neural network-first principles approach to process modeling, AIChE J. 38 (1992) 1499–1511, https://doi.org/10.1002/aic.690381003.

[12] M.S.P. Rangi, J.S.I. Kwon, Deep hybrid modeling of chemical process: application to hydraulic fracturing, Comput. Chem. Eng. 134 (2020), https://doi.org/10.1016/j.compchemeng.2019.106696.

[13] L. Rajulapati, S. Chitra, B. Shyamala, R. Ranganvanvi, Integration of machine learning and first principles models, AIChE J 68 (2022) 1–17, https://doi.org/10.1002/aic.17715.

[14] D. Machalek, J. Tuttle, K. Anderson, R.M. Powell, Dynamic energy system modeling using hybrid physics-based and machine learning encoder–decoder models, Energy AI 9 (2022) 100172, https://doi.org/10.1016/j.egyai.2022.100172.

[15] D. Lee, A. Jayaraman, J.S. Kwon, Development of a hybrid model for a partially known intracellular signaling pathway through correction term estimation and neural network modeling, PLoS Computational Biology 16 (12) (2020) e1008472, https://doi.org/10.1371/journal.pcbi.1008472.

[16] A. Mukherjee, D. Bhattacharyya, On the development of steady-state and dynamic mass-constrained neural networks using noisy transient data, Comput. Chem. Eng. 187 (2024) 108722, https://doi.org/10.1016/j.compchemeng.2024.108722.

[17] M.S.P. Rangi, K. Kan, J-S-I. Kwon, Physics-informed neural networks for hybrid modeling of lab-scale batch fermentation for β-carotene production using Saccharomyces cerevisiae, Chem. Eng. Res. Des. 179 (2022) 413–423, https://doi.org/10.1016/j.cherd.2022.01.041.

[18] A. Mukherjee, D. Bhattacharyya, Development of steady-state and dynamic mass and energy constrained neural networks for distributed chemical systems using noisy transient data, Ind. Eng. Chem. Res. 62 (2023) 14211–14229, https://doi.org/10.1021/acs.iecr.3c01429.

[19] M. Raissi, P. Perdikaris, G.E. Karniadakis, Physics-informed neural networks: a deep learning framework for solving forward and inverse problems involving nonlinear partial differential equations, J. Comput. Phys. 378 (2019) 686–707, https://doi.org/10.1016/j.jcp.2018.10.045.

[20] J. Yu, N. Petersen, P. Liu, Z. Li, M. Wirsum, Hybrid modeling and simulation of thermal systems of in-service power plants for digital twin development, Energy 260 (2022) 125088, https://doi.org/10.1016/j.energy.2022.125088.

[21] Z. Cui, J. Xu, W. Liu, H. Zhao, S. Xia, Data-driven modeling-based digital twin of supercritical coal-fired boiler for metal temperature anomaly detection, Energy 278 (2023) 127999, https://doi.org/10.1016/j.energy.2023.127999.

[22] J.P. Sgnini, P.J. Smith, S.T. Smith, Aitlekan Digital Twin: Machine learning in a biomas energy system, Appl. Energy 310 (2022) 118486, https://doi.org/10.1016/j.apenergy.2021.118436.

[23] W. Bradley, J. Kim, Z. Kilwein, L. Blakely, M. Eydenberg, J. Jalvin, C. Laird, F. Boukouvala, Perspectives on the integration between first-principles and data-driven modeling, Comput. Chem. Eng. 166 (2022) 107898, https://doi.org/10.1016/j.compchemeng.2022.107898.

[24] A. Chakraborty, S. Saraswti, M. Claussen, V. Venkatasubramanian, Hybrid ai models in chemical engineering-a purpose-driven perspective, Computer Aided Chemical Engineering 51 (2022) 1307–1312, https://doi.org/10.1016/B978-0-323-95879-0.50232-6.

[25] S. Zendehboudi, N. Rezaei, A. Lohi, Applications of hybrid models in chemical, petroleum, and energy systems: a systematic review, Appl. Energy 228 (2018) 2539–2566, https://doi.org/10.1016/j.apenergy.2018.06.051.

[26] Y. Chen, M. Ierapetritou, A framework of hybrid model development with identification of plant-model mismatch, AIChE J 66 (2020) 1–16, https://doi.org/10.1002/aic.16996.

[27] D.S. Lee, P.A. Vanrolleghem, M.P. Jong, Parallel hybrid modeling methods for a full-scale cokes wastewater treatment plant, J. Biotechnol. 115 (2006) 317–328, https://doi.org/10.1016/j.jbiotec.2004.09.001.

[28] A. Ozmen, Y.Y. Chen, H. Parker, D.S. Mebane, C.O. Okoli, A. Lee, A. Tong, L-S. Fan, L.T. Biegler, A.P. Burgard, D.C. Miller, D. Bhattacharyya, Kinetic model development and Bayesian uncertainty quantification for the complete reduction of Fe-based oxygen carriers with CH4, CO, and H2 for chemical looping combustion, Chem. Eng. Sci. 292 (2022) 117912, https://doi.org/10.1016/j.ces.2022.117912.

[29] M. von Stosch, R. Oliveira, J. Peres, S. Feyo de Azevedo, Hybrid semi-parametric modeling in process systems engineering: Past, present and future, Comput. Chem. Eng. 60 (2014) 86–101, https://doi.org/10.1016/j.compchemeng.2013.08.008.

[30] L.T. Biegler, Nonlinear programming: concepts, algorithms, and applications to chemical processes, Society for Industrial and Applied Mathematics, 2010, https://doi.org/10.1137/1.9780898719383.

[31] J. Cochran, M. Miller, O. Zinaman, M. Milligan, D. Arent, B. Palmintier, M. O'Malley, S. Mueller, E. Lannoye, A. Tuohy, B. Kujala, M. Sommer, M. Holttinen, J. Kiviluoma, S.K. Soonee, Flexibility in 21st Century Power Systems, National Renewable Energy Laboratory (NREL), Golden, CO (United States), 2014. https://doi.org/10.2172/1130520.

[32] N. Kumar, P. Besuner, S. Lefton, D. Agan, D. Hilleman, Power Plant Cycling Costs, National Renewable Energy Laboratory (NREL), Golden, CO (United States), 2012. https://doi.org/10.2172/1046036.

[33] Y. Wang, D. Bhattacharyya, R. Turton, Evaluation of novel configurations of natural gas combined cycle (NGCC) power plants for load-following operation using dynamic modeling and optimization, Energy Fuels 34 (2020) 1053–1070, https://doi.org/10.1021/acs.energyfuels.0c03036.

[34] Y. Wang, D. Bhattacharyya, R. Turton, Multiobjective dynamic optimization for optimal load-following of natural gas combined cycle power plants under stress constraints, Ind. Eng. Chem. Res. 60 (2021) 14231–14270, https://doi.org/10.1021/acs.iecr.1c01582.

[35] K. Hedrick, B. Oneill, S.E. Zitney, D. Bhattacharyya, Development of a health monitoring framework: application to a supercritical pulverized coal-fired boiler, Energy 290 (2024) 130153, https://doi.org/10.1016/j.energy.2023.130153.

[36] Q.M. Le, J. Ha, D. Bhattacharyya, S.E. Zitney, A.P. Burgard, Design and multiobjective dynamic optimization of superheaters for load-following operation in pulverized coal power plants, Ind. Eng. Chem. Res. 63 (2024) 830–844, https://doi.org/10.1021/acs.iecr.3c02230.

[37] J. Qi, K. Zhou, J. Huang, X. Si, Influence of temperatures on the oxide spallation of T91 alloy superheater tubes in power plant, Appl. Therm. Eng. 128 (2018) 244–252, https://doi.org/10.1016/j.applthermaleng.2017.08.139.

[38] A.S. Sabau, I.G. Wright, J.P. Shingledecker, Oxide scale exfoliation and regrowth in T91/T92 superheater tubes, Mater. Corros. 63 (2012) 896–908, https://doi.org/10.1002/maco.201206405.

[39] L.J. Mendes, N.B. Barros, J. Yoze Azevedo, Thermal conductivity analysis of an ash deposit on boiler superheater, Powder Technol. 318 (2017) 329–336, https://doi.org/10.1016/j.powtec.2017.06.005.

[40] J. Qi, K. Zhou, J. Huang, X. Si, Numerical simulation of the heat transfer of superheater tubes in power plants considering oxide scale, Int. J. Heat Mass Transf. 122 (2018) 929–938, https://doi.org/10.1016/j.ijheatmasstransfer.2018.01.119.

[41] C.D. Somarajula, D. Bhattacharyya, S. Hu, X. Liu, Hot corrosion monitoring in boilers using a nonlinear estimator and electrochemical noise-based corrosion sensors, Ind. Eng. Chem. Res. 63 (2024) 994–1009, https://doi.org/10.1021/acs.iecr.3c03842.

[42] Y. Cai, K. Tay, Z. Zheng, W. Yang, H. Wang, G. Zang, Z. Li, S. Kang Boon, P. Subhash, Modeling of ash formation and deposition processes in coal and biomass fired boilers: a comprehensive review, Appl. Energy 230 (2018) 1447–1544, https://doi.org/10.1016/j.apenergy.2018.08.084.

[43] K. Hedrick, K. Hedrick, B. Oneill, S.E. Zitney, D. Bhattacharyya, Dynamic modeling, parameter estimation, and data reconciliation of a supercritical pulverized coal-fired boiler, Ind. Eng. Chem. Res. 61 (2022) 16764–16779, https://doi.org/10.1021/acs.iecr.2c01977.

[44] C. De Michelis, C. Rinaldi, C. Sampietri, R. Varin, Condition monitoring and assessment of power plant components, in: Power Plant Life Management and Performance Improvement, Woodhead Publishing, 2011, pp. 28–109, https://doi.org/10.1533/9780857092854.1.28.

[45] C.D. Somarajula, State Estimation and Economic Analysis for Electrochemical Sensor-Based Corrosion Monitoring, Graduate Theses, Dissertations, and Problem Reports (2024), https://doi.org/10.33915/etd.12371.

[46] A. Hamid, A.M. Hasan, S.N. Azhari, Z. Marin, Z.A. Putra, Hybrid modelling for remote process monitoring and optimisation, Digital Chem. Eng. 4 (2022) 100044, https://doi.org/10.1016/j.dche.2022.100044.

[47] L.M. Romeo, R. Gareta, Hybrid System for fouling control in biomass boilers, Eng. Appl. Artif. Intel. 19 (2006) 913–925, https://doi.org/10.1016/j.engappai.2006.01.019.

[48] K. Magdouli, R. Tachrimoh, F. Cinnella, Application of machine learning to enhance the performance of a two-stage, two-temperature ejector cycle driven by the waste heat of exhaust gas, Energy. Convers. Manage. X12 (2024) 118361, https://doi.org/10.1016/j.enconman.2024.118361.

[49] D. Santos, S. Costa, L. Reis, T. Gonçalves, I. Malico, P. Canhoto, F. Alvarez, M. Barão, A grey-box Neural Network Composite Model for an Industrial Heating Furnace, in: 25th Portuguese Conference on Pattern Recognition RECPAD2019, 2019, pp. 85–85.

[50] A. Chaibakhsh, Modelling and long-term simulation of a heat recovery steam generator, Math. Comput. Model. Dyn. Syst. 19 (2013) 91–114, https://doi.org/10.1080/13873954.2012.686422.

[51] A. Aminzadeh, A.A. Safavi, A.R. Saifi, Development of a hybrid simulator of a fossil fuel steam power plant, in: 2003 European Control Conference (ECC), IEEE, 2003, pp. 1905–1910, https://doi.org/10.23919/ECC.2003.7085244.

[52] M. Rusinovich, V. Stanek, Hybrid model of steam boiler, Energy 25 (2010) 1107–1115, https://doi.org/10.1016/j.energy.2009.06.004.

[53] T. Barszcz, P. Czop, Estimation of feedwater heater parameters based on a grey-box approach, Int. J. Appl. Math. Comput. Sci. 21 (2011) 709–719, https://doi.org/10.2478/v10006-011-0056-6.

[54] T. Barszcz, P. Czop, J. Madura, Model-based evaluation of a power plant steam boiler system, Problemy Eksploatacji 2 (2011) 7–19.

[55] A.A. Farooq, A. Afram, N. Schulz, F. Janabi-Sharifi, Grey-box modeling of a low pressure electric boiler for domestic hot water system, Appl. Therm. Eng. 84 (2015) 257–267, https://doi.org/10.1016/j.applthermaleng.2015.03.030.

[56] D. Bashir, V. Saini, O. Bhattacharyya, S. Saadiman, C. Boohaker, Estimation-based model predictive control with objective prioritization for mutually exclusive objectives: application to a power plant, J. Process Control 141 (2024) 103268, https://doi.org/10.1016/j.jprocont.2024.103268.

[57] Y. Shi, T. Han, F. Cai, J. Wei, J. Jia, S. Fang, A hybrid prediction approach for enhancing heat transfer efficiency of coal-fired power plant boiler, Energy Rep. 9 (2023) 648–668, https://doi.org/10.1016/j.egyr.2023.01.127.

[58] Y. Zhao, Y. Cai, H. Jiang, Recurrent neural network-based hybrid modeling method for digital twin of boiler system in coal-fired power plant, Appl. Sci. 13 (2023) 4905, https://doi.org/10.3390/app13084905.

[59] P. Wang, F. Ni, Y. Cai, Z. Zhao, X. Fan, Prediction of superheated steam temperature for thermal power plants using a novel integrated method based on the hybrid model and attention mechanism, Appl. Therm. Eng. 209 (2022) 117899, https://doi.org/10.1016/j.applthermaleng.2022.117899.

[60] Q. Wang, L. Fan, K.Y. Lee, Z. Wu, Deep-learning modeling and control optimization framework for intelligent thermal power plants: a practice on superheated steam temperature, Korean J. Chem. Eng. 38 (2021) 1983–2002, https://doi.org/10.1007/s11814-021-0860-6.

[61] S. Prasanth, S. Narayanan, V. Sivakumaran, R.S. Sharanya Ponniwa, A hybrid technique to control superheater steam temperature in power plants using multi modeling and predictive sliding mode control, Sustain. Energy Technol. Assess. 59 (2023) 102912, https://doi.org/10.1016/j.seta.2022.102912.

[62] W. Zima, S. Grądziel, A. Cebula, M. Kerak, R. Kozak-Jagieła, M. Pilarczyk, Mathematical model of a power boiler operation under rapid thermal load changes, Energy 262 (2023) 125634, https://doi.org/10.1016/j.energy.2022.125634.

[63] P. Sarda, E. Hedrick, K. Reynolds, D. Bhattacharyya, S.E. Zitney, B. Omell, Development of a dynamic model and control system for load-following studies of supercritical pulverized coal power plants, Processes 6 (2018) 220, https://doi.org/10.3390/pr6110220.

[64] F. Shah, M.Z. Shariff, M.S.P. Rangi, C. Stavrakis, J.S.I. Kwon, C. Botre, J. Mishra, Deep neural network-based hybrid modeling and experimental validation for an industry-scale fermentation process: identification of time-varying dependencies among parameters, Chem. Eng. J. 441 (2022) 135943, https://doi.org/10.1016/j.cej.2022.135643.

[65] N. Shapurs, J. Sarg-El Kwon, Introducing hybrid modeling with time-series-transformer: a comparative study of series and parallel approach in batch crystallization, Ind. Eng. Chem. Res. (2023), https://doi.org/10.1021/acs.iecr.3c03624.

[66] Y.M. Chiang, L.C. Chang, F.J. Chang, Comparison of static-feedforward and dynamic-feedback neural networks for rainfall-runoff modeling, J. Hydrol. 290 (2004) 297–311, https://doi.org/10.1016/j.jhydrol.2003.12.033.

[67] M.M. Mejari, M. Khanra, A systematic review on overfitting control in shallow and deep neural networks, Springer Netherlands, 2021, https://doi.org/10.1007/s10462-021-09975-1.

[68] J. Manikandan, K.V. Naidu, B. Janardhan, M.R. Kishore, K. Prabhakar, Comparison of static and dynamic neural network models in predicting outlet temperature of shell and tube heat exchanger, Int. J. Vehicle Struct. Syst. 11 (2019) 585–588, https://doi.org/10.4273/ijvss.11.5.22.

[69] A. El-Shafie, Dynamic versus static neural network model for rainfall forecasting at Klang River Basin, Malaysia, Hydrol. Earth Syst. Sci. Discuss. 8 (2011) 6489–6532, https://doi.org/10.5194/hessd-8-6489-2011.

[70] Y.M. Ran, M.S. Alhajeri, J. Luo, S. Chen, F. Abdullah, Z. Wu, P.D. Christofides, A tutorial review of neural network modeling approaches for model predictive control, Comput. Chem. Eng. 165 (2022) 107956, https://doi.org/10.1016/j.compchemeng.2022.107956.

[71] Y. Yu, X. Si, C. Hu, J. Zhang, A review of recurrent neural networks: LSTM cells and network architectures, Neural Comput. 31 (2019) 1235–1270, https://doi.org/10.1162/neco_a_01199.

[72] M. Schoukens, K. Tiels, Identification of block-oriented nonlinear systems starting from linear approximations: a survey, Automatica 85 (2017) 272–292, https://doi.org/10.1016/j.automatica.2017.06.044.

[73] J. Ma, P. Mahapatra, S.E. Zitney, L.T. Biegler, D.C. Miller, D.-R.-Al. Builder, A software tool for generating fast and accurate nonlinear dynamic reduced models from high-fidelity models, Comput. Chem. Eng. 84 (2016) 60–74, https://doi.org/10.1016/j.compchemeng.2014.07.021.

[74] K. Hammar, T. Djärnah, N. Bettaveh, Nonlinear system identification using fractional Hammerstein-Wiener models, Nonlinear Dyn. 98 (2019) 2327–2338, https://doi.org/10.1007/s11071-019-04931-9.

[75] K.-L. Du, M.N.S. Swamy, Neural Networks and Statistical Learning, Springer London, London, 2014, https://doi.org/10.1007/978-1-4471-5571-3.

[76] M.T. Siegelmann, B.G. Horne, C.L. Giles, Computational capabilities of recurrent NARX neural networks, IEEE Trans. Syst. Man Cybern. B Cybern. 27 (1997) 208–215, https://doi.org/10.1109/3477.558801.

[77] Z. Boussaada, O. Curea, A. Remaci, H. Camblong, N.M. Bellaaj, A nonlinear autoregressive exogenous (NARX) neural network model for the prediction of the daily direct solar radiation, Energies 11 (2018), https://doi.org/10.3390/en11030620.

[78] S.L. Brunton, J.L. Proctor, J.N. Kutz, Discovering governing equations from data by sparse identification of nonlinear dynamical systems, Proceedings of the national academy of sciences 113 (15) (2016) 3932–3937, https://doi.org/10.1073/pnas.1517384113.

[79] Á. Cored, H.V. Sahinidis, D.C. Miller, Learning surrogate models for simulation-based optimization, AIChE J 60 (2014).

[80] W. Sun, R.D. Braatz, ALVEN: Algebraic learning via elastic net for static and dynamic nonlinear model identification, Comput. Chem. Eng. 143 (2020) 107123, https://doi.org/10.1016/j.compchemeng.2020.107103.

[81] K. Yavari, S. Shukla, R.N. Arya, Heat exchanger network design using MATLAB, Chem Eng & Technol 43 (2022) 908–916, https://doi.org/10.1002/ceat.202100543.

[82] L.F. Shampine, M.W. Reichelt, The MATLAB ODE Suite, SIAM J. Sci. Comput. 18 (1997) 1–22, https://doi.org/10.1137/S1064827594276424.

[83] A. Lazrak, F. Boukelsem, S. Bonnet, O. Fraisa, A. Lacoste, F. Papillon, B. Souyri, Development of a dynamic artificial neural network model of an absorption chiller and its experimental validation, Renew. Energy 96 (2016) 1059–1072, https://doi.org/10.1016/j.renene.2016.05.033.

[84] J. Kim, M. Lee, J. Yu, J. Jang, J. Yoo, J.M. Park, S. Kim, Data-driven approach to attemperator steam temperature prediction in biomass power plant, J. Electr. Eng. Technol. 14 (2019) 1423–1432, https://doi.org/10.1007/s42835-019-00177-x.

[85] J.M. Ferguson, M.L. Tager, R. Zand-Ferguson, M. Jastenisk, B.D. Marxvell, Incorporating parameter estimability into model selection, Front. Ecol. Evol. 7 (2019) 1–13, https://doi.org/10.3389/fevo.2019.00427.